# *Chapter 4*

## Design, Synthesis and Characterization of benzimidazole based amide and urea derivatives as Supramolecular gelators

## 4.1 Introduction

LMWGs (Low Molecular Weight Gelators), a smart material with fascinating applications such as Anion sensing[1–4], environmental remediations[5], templated directed nanostructures, catalysis[6], biomedical applications[7] and response to the external stimuli like light, pH, heat and cations[8].

Over a past decade perusing the literature, it was uncovered that these gelators mainly consist of long fatty acids[9], amides, urea[10], carbohydrates, nucleobases[11], steroids[9], oligopeptides[12] and dendrimers[13]. It was soon realized that Hydrogen-bonding plays important role in the gelation mechanism, as among all the functionalities amide and urea are extensively used scaffold for the design of supramolecular gels. Amide consist of carbonyl oxygen as hydrogen bond acceptor and presence of N-H hydrogen readily makes it donor which increase the intermolecular interaction[14], whereas urea includes self-complementary hydrogen bonds between oxygen(C=O) and N-H hydrogens which forms directional assembly[10,15] as shown in the scheme 4.1.

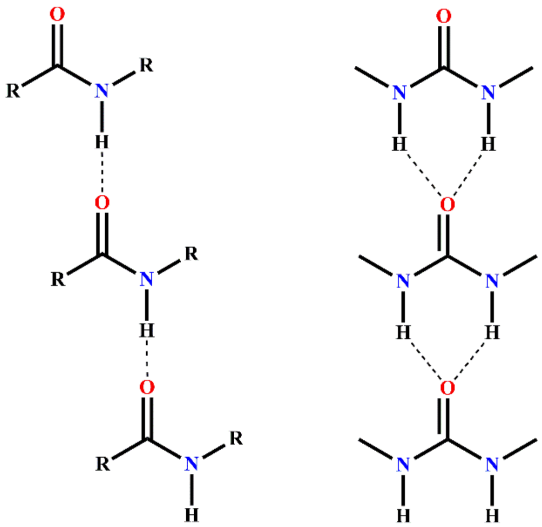

*Scheme 4.1 Hydrogen bonding network of amide and urea*

Furthermore, among the different gelators prepared, benzimidazole draw attention due to availability of N-H or polar C-H bonds for hydrogen bonding and charge-charge interaction with the ionic species. Also, the benzimidazole structures have π-stacking ability, which is advantageous during molecular aggregation. Benzimidazole derivatives are widely chosen as a multifunctional unit for the synthesis of bioactive organic compounds because of their structural similarities to the natural nucleotides[16]. Various reports has been put forward that consist benzimidazole unit to recognize or remove the different analytes from the solution[17,18]. In this regard it was found that there are very few reports of supramolecular gelator based on benzimidazole derivatives[19,20].

In this work, we have synthesized the benzimidazole based compounds consisting of varying alkyl chain functionalized along with the uni-directional H-bond forming groups (amide and urea). Efforts were also directed to understand the role of two different hydrogen bonded supramolecular assemblies on the gelation of various solvents by two classes of LMWGs (bisamide- and bisurea) gelators (Scheme 4.2). Moreover, it is further probed the role of different solvents effect on LMWGs containing different H-bond groups. Both sets of LMWGs have similar molecular scaffolds, making them an excellent tool for determining the relative importance of the supramolecular interactions involved in the gelation process. Total six compounds were synthesized with the fixed hydrophilic part(benzimidazole) and varying hydrophobic alkyl chain (tridecyl, pentadecyl and heptadecyl) with urea and amide linker. Generally, this types molecule presumed to be gelate the solvent by two different types of interactions van der Waals interactions and Hydrogen bonding and synergistic effects of these interactions results in gelation[21]. Gelation behaviour and stability of this compounds was analysed in different solvent and solvents mixtures, gels are investigated with various physicochemical techniques. Also, this study will provide an opportunity to understand how H-bonding groups such as amide and urea, influence the gelation behaviour, if the LMWGS back bone is unaltered. Moreover, the anion sensing capability of this compounds was also probe. Solvent parameter studies were performed to get an idea about the effect of solvent properties on gelation behaviour.

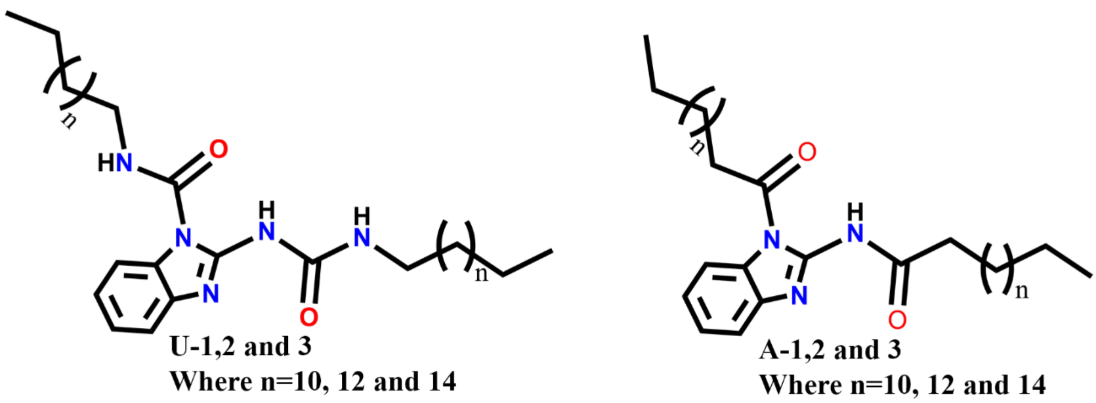


***Scheme 4.2*** *Chemical structure of compounds synthesized*

## 4.2 Materials and Physical measurements

### 4.2.1 Materials

Long chain aliphatic carboxylic acids and 2-aminobenzimidazole were purchased from Sigma Aldrich. Oxalyl chloride, Diphenylphosphoryl azide and triethylamine were obtained from CDH (P) Ltd., India and used without any further purification. Solvents for gelation studies were reagent grade and used without any distillation. Further solvents for synthesis were purified and dried over molecular sieve.

### 4.2.3 Rheological studies

The rheology studies of the organogels (at MGC value) were recorded using TA Instruments ARES G2 Rheometer. Amplitude sweep was performed at room temperature (23˚C) using 50 mm parallel plates maintained at a gap of 1 mm with a frequency variation of 10 rad/sec.

### 4.2.4 NMR Spectroscopy

NMR spectra of Compound was recorded in $CDCl_3$ on BRUKER ADVANCE, 400MHz Spectrometer at 298 kelvin temperature.

### 4.2.5 FT-IR Spectroscopy

FT-IR Studies of Compounds and its xerogel were performed in solid-state using KBr pellet on BRUKER ALPHA FT-IR Spectrometer and spectra were recorded in the wavenumber range from 400-4000 $cm^{-1}$.

### 4.2.6 SEM Measurements

Hot solution of gelator in respective solvents was placed on sample holder and allowed to cool to form gel, and then dried under vacuum. Dried gel was subjected to gold sputtering using POLARON SC7620 Sputter Coater and this gold coated dried gel was subjected to JEOL JSM 5610 LV SEM instrument after carbon coating.

### 4.2.7 Powder X-ray Diffraction

Powder XRD pattern of the neat gelator (Bulk) and xerogel (obtained from slow evaporation) was obtained from X'pert Pan Analytical Powder diffractometer with Cu Kα (1.54 Å) radiation (45 kV, 40 mA). The proportional counter detector collected over the range of $2\theta$=10-50°.

### 4.2.8 UV-Visible Spectroscopy studies

The electronic spectra (in THF at room temperature) in the range of 200-600 nm were recorded on a model JASCO 7600 UV-VIS spectrophotometer.

### 4.2.9 Fluorescence study

Fluorescence spectra were recorded on a JASCO FP-6300 fluorescence spectrophotometer.

### 4.2.10 Small angle Neutron scattering

Small-angle neutron scattering experiments were performed on the SANS diffractometer at Guide Tube Laboratory, Dhruva Reactor, Bhabha Atomic Research Centre, Mumbai, India [22]. In SANS, one measures the coherent differential scattering cross-section ($d\Sigma/d\Omega$) per unit volume as a function of wave vector transfer Q (=$4\pi \sin\theta/\lambda$, where k is the wavelength of the incident neutrons and $2\theta$ is the scattering angle). The mean wavelength of the monochromatized beam from the neutron velocity selector is 5.2 Å with a spread of $\Delta\lambda/\lambda \sim 15\%$. The angular distribution of neutrons scattered by the sample is recorded using a 1 m long one-dimensional $He^3$ position-sensitive detector. The instrument covers a Q-range of 0.015–0.26 $Å^{-1}$.

## 4.3 Experimental procedures

### 4.3.1 Gelation Studies

Gelation studies of the synthesized compound were carried out by taking a weighted amount (10 mg) of a powdered compound in the known amount of solvent (0.5 mL), and the mixture was heated until the dissolution of the powder in the oil/water bath, till the complete dissolution of the solid compound. The resultant solution was kept for half an hour to cool down at 25 ˚C and the immobilization of the solvent was tested by inverting the vial upside down. The free-flowing clear system is considered as ‘‘S” (soluble), the compound which is soluble on heating, but crystallizes and precipitates on cooling is termed as ‘‘C” (crystallization) and ‘‘P” (precipitation) and immobilization of solvent (Observed when the vial was inverted) is denoted as ‘‘G”. The MGC (Minimum Gelator Concentration) for each gel/solvent system is determined by a gradual increase in the solvent by 0.5 mL till the gelation is observed. The weighted amount of solvent/compounds are used for the determination of solvent gelled by the compounds. The gel strength or sol–gel transition temperature ($T_{gel}$) was determined by gradual heating (0.5˚C per minute) of the vial containing gel (at MGC value in 1 mL solvent) using 'ball-drop-method' and 'inverted vial method'. Each experiment is repeated at least 3 times to get the average $T_{gel}$ value for a given solvent/gelator system.

### 4.3.2 Absorption studies

The stock solution of A2 and U2 (50 μM) was prepared and the stock solution of various anions (12.4 mM) (Tetrabutylammonium salts of Fluoride, Bromide and Dihydrogenphosphate) and metal salts [Lead ($Pb^{2+}$), Cadmium ($Cd^{2+}$), Cobalt ($Co^{2+}$), Mercury ($Hg^{2+}$) and Manganese ($Mn^{2+}$)] with concentration 12.4 mM were prepared in Tetrahydrofuran (THF). The calculated amount of stock solution of anion and metal salts was added to the 2.5 mL of compound-1 solution to get the required concentration of anion to carry out spectroscopic analysis.

### 4.3.3 Emission studies

The stock solution of A2 and U2 (50 μM) was prepared and the stock solution of various anions (12.4 mM) (Tetrabutylammonium salts of Fluoride, Bromide and Dihydrogenphosphate) and metal salts [Lead ($Pb^{2+}$), Cadmium ($Cd^{2+}$), Cobalt ($Co^{2+}$), Mercury ($Hg^{2+}$) and Manganese ($Mn^{2+}$)] with concentration 12.4 mM were prepared in Tetrahydrofuran (THF). The calculated amount of stock solution of anion and metal salts was added to the 2.5 mL of compound-1 solution to get the required concentration of anion to carry out analysis.

### 4.3.4 Job plot

Continuous variation method was used to determine the stoichiometry of the host guest complex. In this method solutions of equal concentration of host and guest are prepared in the appropriate solvent. After that, solution of host and guest were mixed with the different proportion maintaining the constant total volume around 3.0 mL. The compositions are 3:0, 2.8:0.2; 2.5:0.5, 2.2:0.8, 2:1, 1.8:1.2, 1.5:1.5, 1:2, 0.8:2.2, 0.5:2.5, and 0.2:2.8 respectively. These solutions are kept for one hour at room temperature with the occasional stirring. The emission spectra of these solutions were taken. The mole fraction of B2 was then plotted against the ($I_0$-I) where '$I_0$' is fluorescence maxima of A2 and 'I' is fluorescence maxima of different solution prepared above. Same procedure was used for U2 respectively.

### 4.3.5 SANS Analysis

The SANS data for gels were analysed employing the traditional two-stage network model of the polymer gels[23–25] comprising two terms described (1)

$$I(Q) = \frac{I(0)}{1+Q^2\xi^2} + \frac{A}{Q^n} + Bkg \qquad (1)$$

where, the first term is a Lorentzian function, called as Ornstein–Zernike equation which describes the scattering caused by the compositional fluctuations, and its Fourier transform gives the correlations. I(0) denotes the forward scattering and ξ is the correlation length (is often described as a blob where the excluded volume effects are observed) of the system.

Since there is no low-*Q* cut-off is observed in the SANS data, it implies that the size of these inhomogeneities is larger than that can be seen in the limited *Q*-range of the instrument. It has been incorporated in the second term which is a power law (depicting the mass fractal dimension) accounting for the large moieties present in the sample.

For mass fractals, the mass $M(r)$ inside a spherical surface with radius $r$ inscribing the structure is given by $M(r)$ α $r^d$, $d \leq 3$ and $S(Q)$ for such fractal structure can be expressed as [26,27]

$$S_{mf}(Q) = 1 + \frac{1}{(QR_b)^{D_m}} \frac{D_m \Gamma(D_m - 1)}{[1+(Q\xi)^{-2}]^{[(D_m-1)/2]}} \times \sin[(D_m - 1)\tan^{-1}(Q\xi)] \qquad (2)$$

where $\Gamma(x)$ is the gamma function of argument $x$. $R_b$ is the building-block size forming the fractal structure. $D_m$ and $\xi$ are the fractal dimension and the correlation length of the fractal network, respectively.

It may be mentioned that the scattering intensity from mass fractal structures is governed by power-law behaviour in a definite Q range, scattering intensity shows linearity $[I(Q) \sim Q^{-\alpha}]$ in profile in the intermediate Q values $(1/\xi < Q < 1/R_b)$.

$$\frac{d\Sigma}{d\Omega}(Q) \sim Q^{-D_m} \qquad \frac{1}{\xi} < Q < \frac{1}{R_b} \quad \text{for mass fractals} \qquad (3)$$

The value of exponent α varies between 1 and 3 for mass fractals.

### 4.3.6 Synthesis

**U1, U2 and U3**: Acid (1 eq. wt., 2 g), triethylamine (2.2 eq. wt.), and diphenylphosphorylazide (1.2 eq. wt.) was dissolved in dry toluene. The solution was refluxed over 3 hours. The solution was kept at 0 ˚C and the suspension of 2-

aminobenzimidazole (0.5 eq. wt.) is added dropwise and stirred for 15 Hours at Room temperature (25 ˚C) and monitored by TLC until completion (Scheme 4.3). The reaction mixture, obtained after completion, was washed with water and saturated $NaHCO_3$ and then with dil. HCl. and dried over $Na_2SO_4$. Finally, compounds were recrystallized from ethyl acetate.

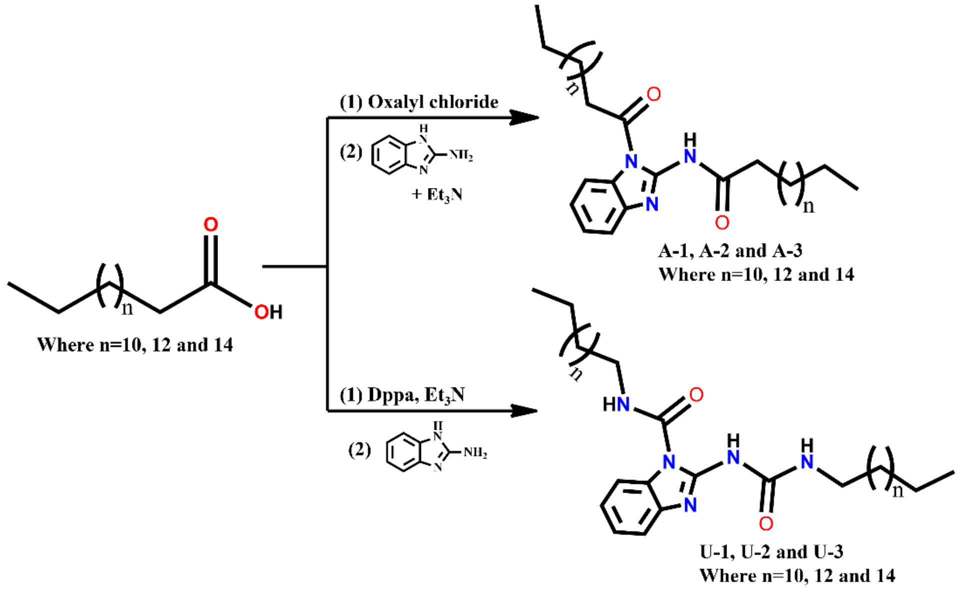


*Scheme 4.3 Preparation scheme for compounds A1 to U3*

**A1, A2 and A3:** Oxalyl chloride (1.5 equivalent) was added to the solution of respective fatty acid (1 equivalent, 2 g) in dry dichloromethane with constant stirring at room temperature under the nitrogen atmosphere. After 12 hours, dichloromethane and excess oxalyl chloride were evaporated under reduced pressure. The acetyl chloride so obtained after the reaction was dissolved in fresh dichloromethane and added slowly to the mixture of 2-aminobenzimidazole (0.5 Eq.) and triethylamine (1.2 equivalent). The solution was stirred under nitrogen atmosphere for 18 hours. The reaction mixture was extracted with ethyl acetate, evaporated in high vacuum and purified by column chromatography over silica gel.

**Analytical Data**

**U1(N-tridecyl-2-(3-tridecylureido)-1H-benzoimidazole-1-carboxamide).**

(1.15 g, Yield 45.4 %) M.P 107 °C $^1$H NMR (400 MHz, $CDCl_3$, TMS): 11.347 (s, 1H, NH), 7.448 (d, 1H; CH), 7.004 (d, 1H; CH), 2.560 -2.522 (t, 2H; $CH_2$), 1.820–1.269(m, 16H, $CH_2$),0.899-0.874 (t, 3H; $CH_3$). MS (EI): m/z 583.8 $[M]^+$. FTIR (KBr): 3353, 3165, 2918, 2850, 1719, 1700, 1619, 1592, 1561, 1472, 1385, 1362, 1217, 1166, 921, 668, 595, $cm^{-1}$.

**U2(N-pentadecyl-2-(3-pentadecylureido)-1H-benzoimidazole-1-carboxamide).** (1.121 g, Yield 48.8 %) M.P 109 °C $^{1}$H NMR (400 MHz, CDCl3, TMS): 11.902 (s, 1H, NH), 10.100-10.074 (d, 1H; NH), 8.378-3.341 (m, 1H; NH), 7.314 -7.066 (m, 4H; CH), 3.485–3.436(q, 2H, $CH_2$), 3.331-3.281 (q, 2H, $CH_2$), 1.717-1.646(q, 2H, $CH_2$), 1.606-1.571 (t, 2H, $CH_2$), 1.571 (s, 47H; $CH_2$), 0.917-0.882 (t, 6H, $CH_3$). MS (EI): m/z 639.9 $[M]^+$. FTIR (KBr): 3424, 2919, 2851, 1719, 1698, 1634, 1618, 1560, 1508, 1471, 1387, 1369, 1221, 1148, 1094, 778, 668 $cm^{-1}$.

**U3(N-heptadecyl-2-(3-heptadecylureido)-1H-benzoimidazole-1-carboxamide).** (1.007 g, Yield 41.2 %) M.P 110 °C $^{1}$H NMR (400 MHz, CDCl3, TMS): 11.908 (s, 1H, NH), 10.083 (d, 1H; NH), 8.369-3.346 (m, 1H; NH), 7.291 -7.124 (m, 4H; CH), 3.491–3.442 (q, 2H, $CH_2$), 3.337-3.286 (q, 2H, $CH_2$), 1.705-1.577 (m, 2H, $CH_2$), 1.280 (t, 47H, $CH_2$), 0.917-0.882 (t, 6H, $CH_3$). MS (EI): m/z 695 $[M]^+$ . FTIR (KBr): 3305, 2919, 2850, 1685, 1633, 1574, 1544, 1469, 1460, 1379, 1274, 1249, 1227, 1058, 728, 536 $cm^{-1}$

**A1(N-(1-tetradecanoyl-1H-benzoimidazol-2-yl)tetradecanamide).** (1.456 g, Yield 60.1 %) M.P 115 °C $^{1}$H NMR (400 MHz, CDCl3, TMS): 12.859 (s, 1H, NH), 11.311(s, 1H, NH), 7.564 (m, 4H; CH), 2.665 -2.627 (t, 6H; $CH_2$), 1.811–1.685(m, 10H, $CH_2$), 1.370-1.260 (m, 36H; $CH_2$), 0.915 (t, 6H, $CH_3$). MS (EI): m/z 553 $[M]^+$ FTIR (KBr): 3380, 2917, 2849, 1681, 1650, 1601, 1587, 1520, 1465, 1360, 1194, 1184, 762, 743, 718, 609, 502 $cm^{-1}$**.**

**A2(N-(1-palmitoyl-1H-benzoimidazol-2-yl)palmitamide).** (1.515 g, Yield 63.8 %) M.P 109 °C $^{1}$H NMR (400 MHz, CDCl3, TMS): 7.269-7.247 (m, 4H, CH), 2.661-2.623 (t, 4H, $CH_2$), 1.787-1.750 ((t, 4H, $CH_2$), 1.265 (m, 48H, $CH_2$), 0.910-0.876 (t, 6H, $CH_3$). MS (EI): m/z 609 $[M]^+$ FTIR (KBr):3381, 2917, 2849, 2678, 1681, 1650, 1601, 1586, 1520, 1464, 1434, 1415, 1312, 1273, 1191, 1037, 896, 848, 762, 742, 718, 609 $cm^{-1}$.

**A3(N-(1-stearoyl-1H-benzoimidazol-2-yl)stearamide).** (1.453 g, Yield 62.10 %) M.P 112 °C $^{1}$H NMR (400 MHz, CDCl3, TMS): 11.151 (s, 1H, NH), 7.564 (m, 4H; $CH_2$), 2.569 -2.531 (t, 2H; $CH_2$), 2.412–2.393(t, 2H, $CH_2$), 1.808-1.682 (m, 4H; $CH_2$), 1.663 (m, 55H, $CH_2$), 0.909 -0.875 (t, 3H, $CH_3$). MS (EI): m/z 666.0 $[M]^+$. FTIR (KBr): 3305, 2919, 2850, 1685, 1633, 1574, 1544, 1460, 1431, 1414, 1379, 1347, 1227, 1110, 1099, 1058, 728, 688, 536, 436 $cm^{-1}$.

## 4.4 RESULTS AND DISCUSSION

### 4.4.1 Gelation studies

*Table 4.1 Gelation profile of compounds*

| | U1 | U2 | U3 | A1 | A2 | A3 |
|---|---|---|---|---|---|---|
| **Heptane** | P | P | P | P | P | P |
| **Hexane** | P | P | P | P | P | P |
| **Pet ether** | P | P | P | P | P | P |
| **Pentane** | P | P | P | P | P | P |
| **Cyclohexane** | P | P | P | P | P | P |
| **$CCl_4$** | P | P | P | P | P | S |
| **Toluene** | P | P | P | P | P | P |
| **Chlorobenzene** | S | S | S | S | S | S |
| **Benzene** | S | S | S | | P | S |
| **DCM** | P | P | P | P | P | S |
| **Isopropanol** | P | I | P | **G (2.4)** | **G (3.4)** | P |
| **Chloroform** | S | S | S | S | S | S |
| **THF** | S | S | S | S | S | S |
| **Ethyl acetate** | P | P | P | **G (1.8)** | **G (3.6)** | P |
| **Nitrobenzene** | P | S | S | P | P | P |
| **Dioxane** | P | P | P | P | P | S |
| **Acetone** | I | I | I | I | I | I |
| **Methanol** | **G (6.2)** | **G (5.3)** | P | P | P | P |
| **Ethanol** | P | **G (3.8)** | P | **G (2.6)** | **G (3.7)** | P |
| **1-propanol** | P | P | P | **G (2.8)** | **G (2.8)** | P |
| **1-butanol** | P | P | P | **G (4.3)** | **G (3.8)** | S |
| **3°-butanol** | P | P | P | P | **G (6.0)** | S |
| **1-pentanol** | P | P | P | **G (2.8)** | **G (3.5)** | S |
| **1-hexanol** | P | P | P | **G (3.5)** | **G (3.6)** | S |
| **2-octanol** | P | S | P | **G (6.9)** | **G (5.6)** | S |
| **1-decanol** | P | P | P | **G (5.1)** | P | P |
| **Glycerol** | P | P | P | P | **G (3.8)** | S |
| **ACN** | P | I | P | **G (1.7)** | **G (1.2)** | **G (2.5)** |
| **Acetic acid** | P | P | P | P | P | S |
| **DMF** | P | P | P | P | P | P |
| **DMSO** | S | P | P | **G (6.2)** | P | **G (5.4)** |
| **Water** | I | I | I | I | I | I |
| **Propane-1,2-diol** | P | P | P | **G (4.4)** | **G (3.5)** | **G (3.1)** |
| **Petrol** | P | P | P | P | P | P |
| **Diesel** | P | P | P | **G (3.9)** | **G (9.2)** | P |
| **Kerosene** | P | P | P | P | P | P |
| **Engine oil** | P | P | P | P | P | P |
| **ACN: water** | P | P | P | P | P | P |
| **THF: water** | P | P | P | P | P | P |
| **Ethanol: water** | P | P | P | P | P | P |
| **Methanol: water** | P | P | P | P | P | P |
| **DMSO: water** | I | I | I | I | I | I |
| **Acetone: water** | I | I | I | I | I | I |
| **IPA: water** | P | P | P | P | P | P |

We examined gelation capability of six novel compounds in 39 pure solvents and five mixture of solvents containing water in the volume ratio of 1:1 respectively and the data was summarized in table 4.1.

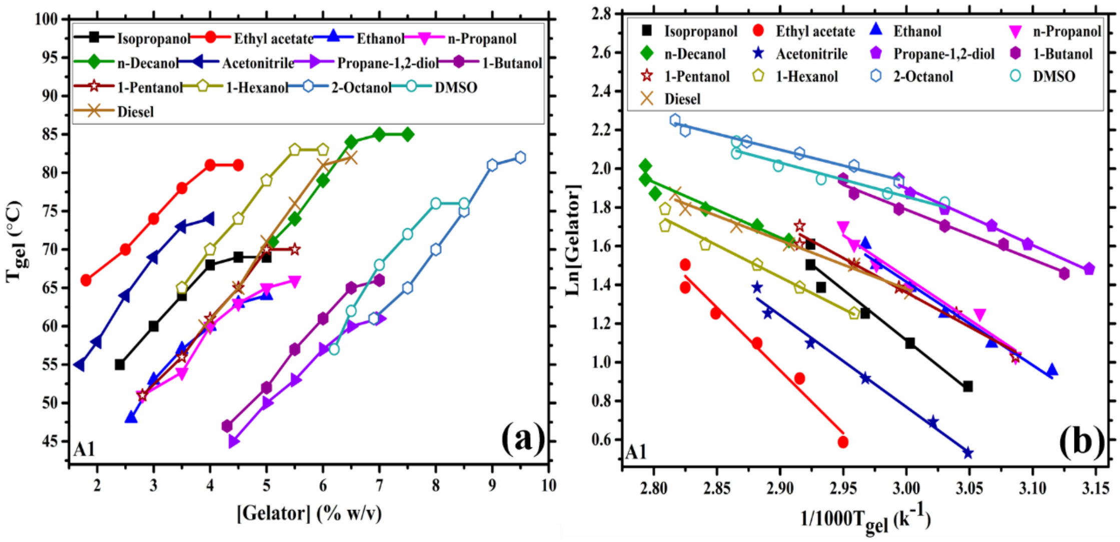


***Figure 4.1*** *Plot of A1 (a) $T_{gel}$ versus gelator concentration (% w/v) (b) Semilog plot of the mole fraction of the gelators against 1/1000 T ($K^{-1}$).*

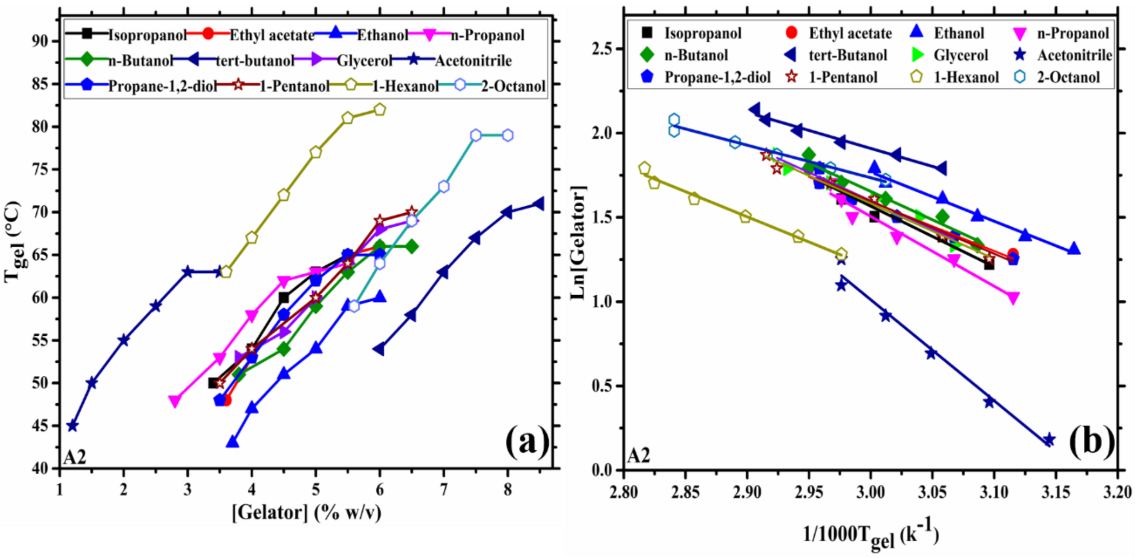


***Figure 4.2*** *Plot of A2 (a) $T_{gel}$ versus gelator concentration (% w/v) (b) Semilog plot of the mole fraction of the gelators against 1/1000 T ($K^{-1}$).*

All the gel so obtained was opaque in nature, thermo-reversible and stable up to months at room temperature. All the compounds were found to be form precipitate in the all the non-polar solvents employed in the study. At the first glance on the gelation table, it was found that gelator (A1 to A3) having the bisamide group are able to gel variety of solvents, mainly the alcohols ranging from ethanol to n-Decanol with the MGC value ranging from 1.5 to 5.1 % w/v.

Further gelation were notably depends upon the alkyl chain length in case of bisamide derivatives owing to the delicate Hydrophobic-hydrophilic balance[28]. Surprisingly compounds containing bisurea functional group are only able to gel two solvents i.e., Methanol and ethanol and U3 found to gel none of the solvents used in the study. Overall, it is apparent that A1, A2 and A3 which contains the bisamide group, gelation occurs only in the polar solvents especially containing alcohols expect in case A3 where gelation is observed only in three solvents and all are tends to precipitate out on cooling in case of non-polar solvents.

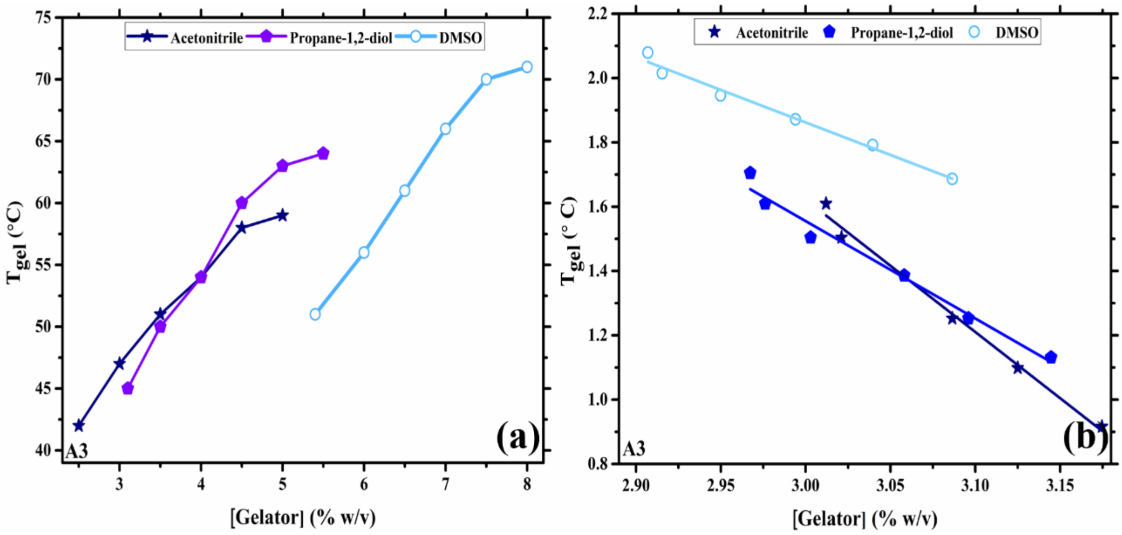


***Figure 4.3*** *Plot of A3 (a) $T_{gel}$ versus gelator concentration (% w/v) (b) Semilog plot of the mole fraction of the gelators against 1/1000 T ($k^{-1}$).*

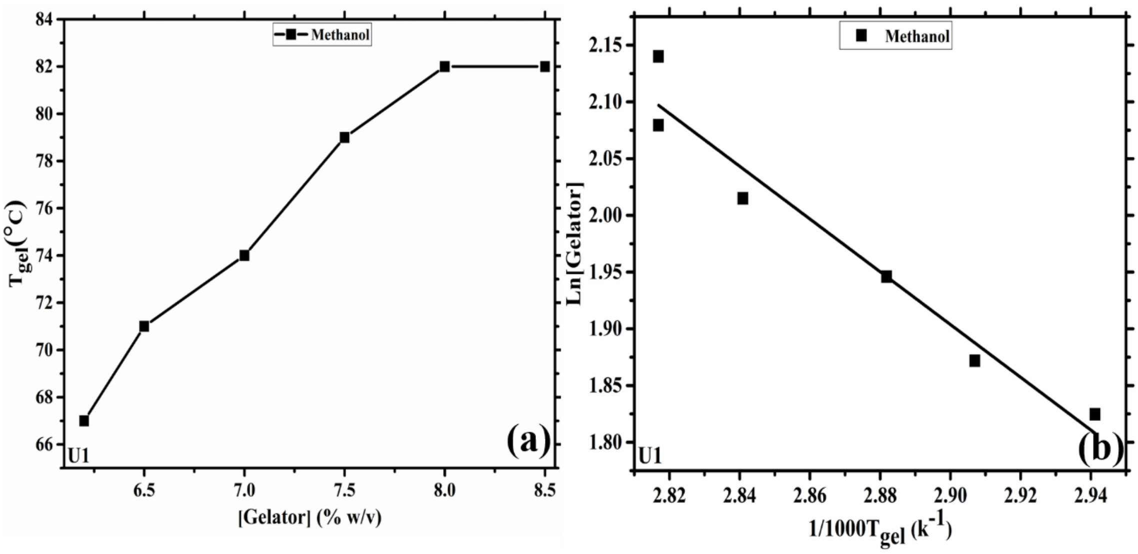


***Figure 4.4*** *Plot of U1 (a) $T_{gel}$ versus gelator concentration (% w/v) (b) Semilog plot of the mole fraction of the gelators against 1/1000 T ($k^{-1}$).*

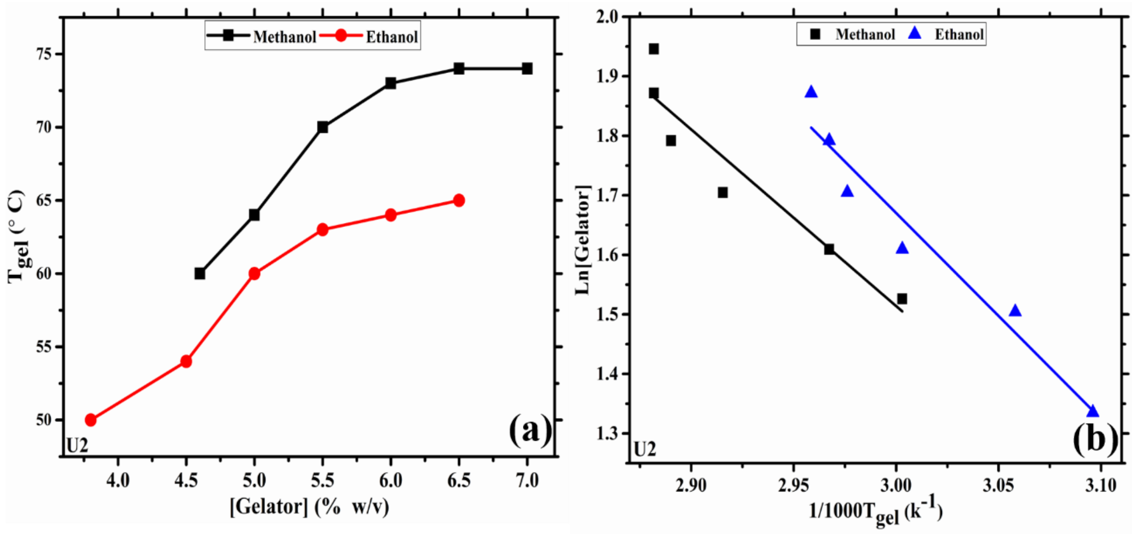


***Figure 4.5** Plot of U2 (a) $T_{gel}$ versus gelator concentration (% w/v) (b) Semilog plot of the mole fraction of the gelators against 1/1000 T ($K^{-1}$).*

In addition, effect of gelator concentration on sol-gel transistion i.e., $T_{gel}$ (Fig 4.1a-4.5a) was also studied and concluded that there is the increase in the $T_{gel}$ values with the increase in the gelator concentration suggested enhancement of thermal stability with increase in the gelation concentration up to some point as similar trends were also reported in the previous work[29,30].

$$Ln[Gelator] = -\left(\frac{\Delta H_m}{RT_{gel}}\right) + Constant \qquad (4)$$

***Table 4.2** $\Delta H_m$ (kJ/mol) obtained from the graph of Semilog plot of the mole fraction of the gelators against 1/1000 T ($K^{-1}$)*

| | U1 | U2 | U3 | A1 | A2 | A3 |
|---|---|---|---|---|---|---|
| **Isopropanol** | - | - | - | 43.32 | 29.33 | - |
| **Ethyl acetate** | - | - | - | 53.94 | 24.39 | - |
| **Methanol** | 19.33 | 24.66 | - | - | - | - |
| **Ethanol** | - | 28.75 | - | 35.82 | 24.21 | - |
| **1-Propanol** | - | - | - | 36.52 | 34.44 | - |
| **1-Butanol** | - | - | - | 21.42 | 28.00 | - |
| **3°-Butanol** | - | - | - | -- | 17.75 | - |
| **1-Pentanol** | - | - | - | 29.52 | 27.29 | - |
| **1-Hexanol** | - | - | - | 27.32 | 24.82 | - |
| **2-Octanol** | - | - | - | 13.59 | 16.07 | - |
| **1-Decanol** | - | - | - | 39.40 | - | - |
| **Acetonitrile** | - | - | - | 28.15 | 49.85 | 34.32 |
| **Prop-1,2-Diol** | - | - | - | 24.44 | 25.97 | 25.18 |
| **Diesel** | - | - | - | 20.92 | - | - |
| **Glycerol** | - | - | - | - | 27.86 | - |
| **DMSO** | - | - | - | 14.63 | - | 16.81 |

Furthermore, semilog of gelator concentration (% w/v) was also plotted against reciprocal of $T_{gel}$ ($k^{-1}$) (Fig 4.1b -4.5b) value and enthalpy of melting ($\Delta H_m$) was extracted from the straight-line graph using Schroeder-Van Laar equation (eqn. 4) and summarized in Table 4.2. In general, increase in chain length of bisamide gelators showed a decrease in the value of $\Delta H_m$, suggested a well packed assembly of molecules with shorted alkyl chain.

## 4.4.2 Solvents effect on gelation

The solvent-gelator intermolecular interactions are equally significant to understanding gelation, even if the gelator-gelator interactions are of utmost relevance[31]. The self-assembly of gelator molecule into their own fibrillar networks is mediated by solvent - gelator interaction, and consequently on solvent characteristics. Thus, solvent parameters study can help us to understand why only few molecules are able to immobilize only particular solvents. Herein, solubility parameters of solvents, ranging from Dielectric constant, dipole moment, refractive index, polarity index, Normalized Dimroth-Reichardt parameter- $E_T^N$, Hildebrand parameter- $\delta_0$[32], Hansen parameters[33] and Kamlet-Taft parameters- α, β, π*[34] are divided into three categories and are correlated with the gelation capability of gelator A2 and A3. All the plots are summarised in Figures 47-58, Supporting Data.

### *Bulk physical polarity scales*

Bulk property of solvents includes, refractive index ($\eta_D$), dipole moment (μ), dielectric constant, and polarity index(P') etc. The ratio of the amount of electrical energy stored in a material by an applied voltage to that stored in vacuum is known as the dielectric constant; the dipole moment results from the non-uniform distribution of atomic charges in a system. The refractive index($\eta_D$) represents the rate of light relative to vacuum in a specific solvent; degree of solvent-solute interactions is given by Polarity index(P'). We found a positive correlation between MGC and refractive index in the case of A1, whereas in A2, the Tgel values were found to increase with increase in refractive index values. There are not many instances reported in literature where refractive index has been found to be related to gelation behaviour. Additionally, a slight negative correlation was observed between the MGC and dipole moment values in case of A2, where the MGC values appeared to decrease with increase in dipole moment. Ideally, an increase in the value of dipole moment can increase the tendency of the solute molecules to get solubilised; in that regard, a solvent with high dipole moment can break the 1D assembly and that with very low value can hinder its interaction with the solute molecules.

***Solvatochromic Parameters***

The Normalized Dimroth-Reichardt parameter, or $E_T^N$, is one of the important parameters to understand all probable intermolecular forces between solvent and solute molecules. In terms of polarizability($\pi^*$), H-bond donating capacity ($\alpha$), and H-bond accepting capacity ($\beta$), a solvent is described by Kamlet-Taft parameters. The capacity of a molecule to gel in a given solvent is known to be correlated with the parameter $\alpha$, the magnitude of $\beta$ affects the stability of the gel and the value $\pi^*$ represents the influence of fiber-to-fiber interactions[35]. In case of A1, there was a positive correlation between MGC and $\beta + \pi^*$ values. We can infer that; the gelation performance was found to be mildly related to the polarizability and hydrogen bond accepting ability of the solvents. No other correlations could be established.

***Thermodynamically derived solvent parameters***

Thermodynamically derived solvent parameters include the Hansen solubility parameters, $\delta_d$, $\delta_p$, $\delta_h$, and $\delta_a$, as well as the Hildebrand parameter($\delta_0$). These parameters depend on the molar Gibbs energy of mixing ($\Delta G_m$), the enthalpy ($\Delta H_m$), or the entropy ($T\Delta S_m$) of either or both components. Hildebrand parameter($\delta_0$), which combines dispersion forces and polar interactions, determines whether or not a solvent will encourage self-assembly[35]. In the case of thermodynamically derived parameters, a correlation between MGC and dispersion interactions, $\delta_d$ could be established. In all the other cases, no major trends could be followed. It is important to emphasize here that, given the high number of solvents studied in this case, correlating the gelation properties with solvent parameters can be demanding. With this study, we have focused our efforts to identify the most appropriate aspects of solvent properties that can potentially affect the gelation behavior in this set of compounds.

### 4.4.3 Rheological studies

To evaluate the mechanical strength of gels, all the gel samples were characterized by rheological measurements. All the gels exhibit clear thixotropic behaviour as G' > G" in all the gels sample consistent with the behaviour shown by of elastic material[36]. As from the references[37], strain sweep experiments can be classified as: Type I (strain softening where G', G" decrease); type II, (strain hardening where G' and G" increase; type III (weak strain overshoot where G' decreases, G" increases followed by decrease) and type IV (strong strain overshoot where G', G" increase followed by decrease).

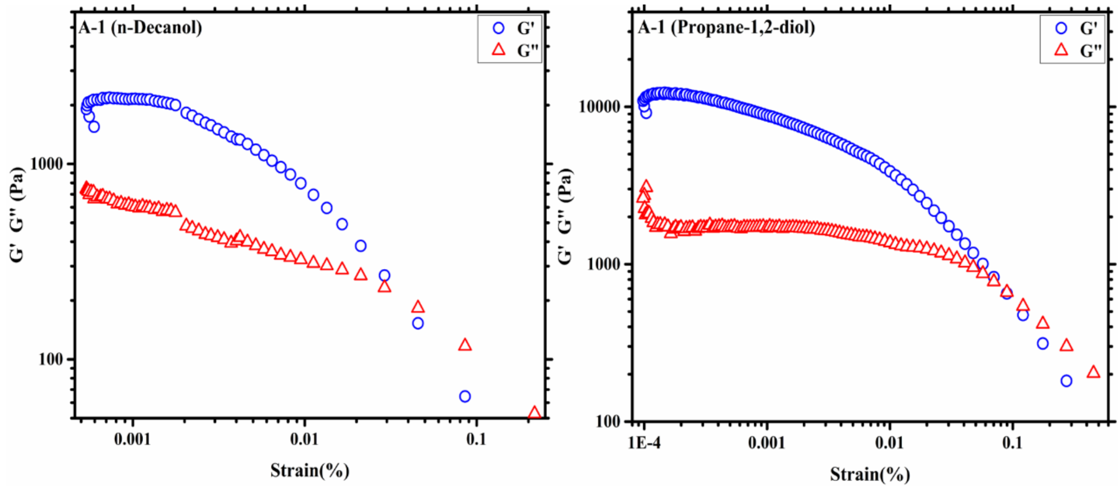


***Figure 4.6*** *Evolution of G' and G" as a function of oscillation strain of A1 in different solvents*

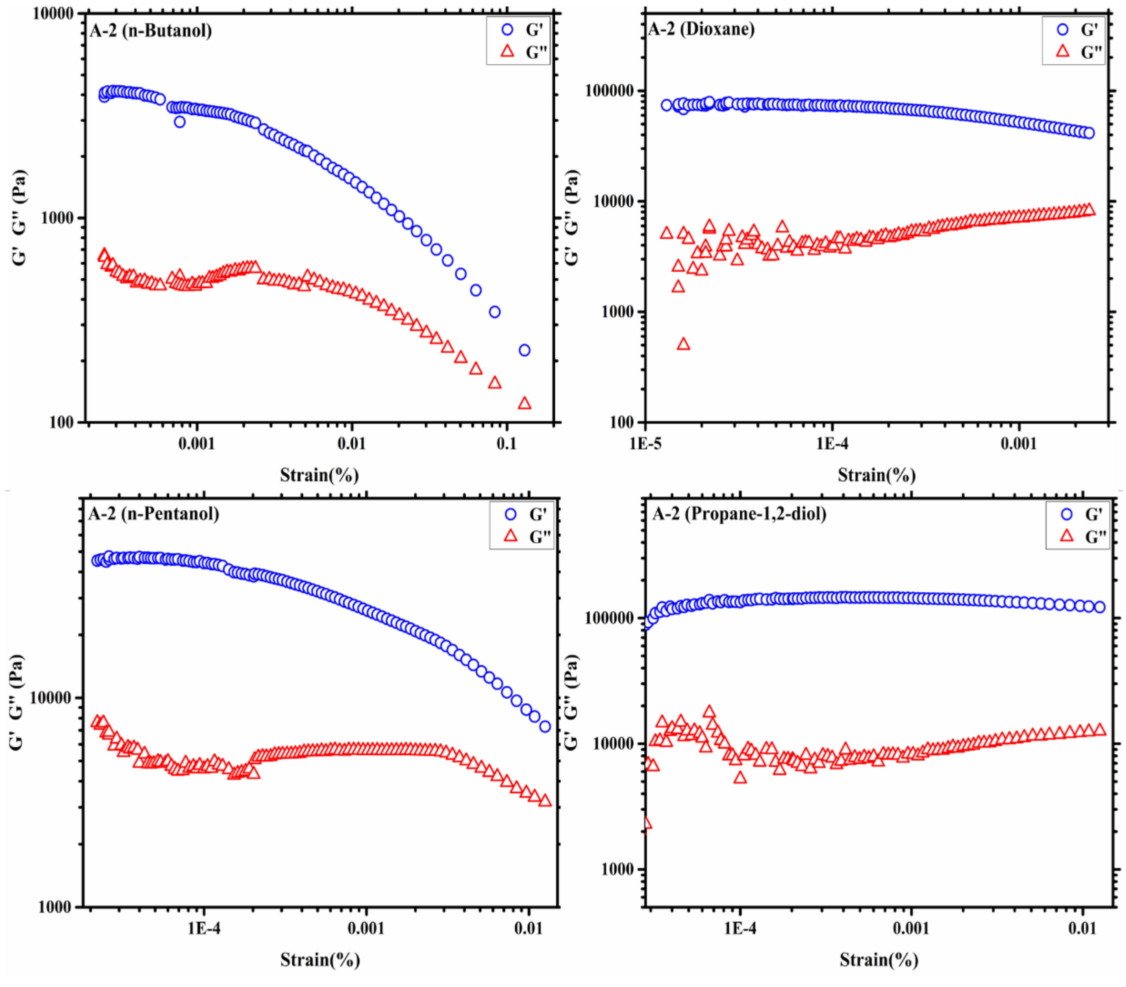


***Figure 4.7*** *Evolution of G' and G" as a function of oscillation strain of A2 in different solvents*

As evident from the Figure 4.6, compound A1 shows decrease in the G’ and G’’ with applied strain classified as Type I, it has been seen that at the beginning values of G’ and G” remain constant until the strain value of 0.018 % and decreasing exponentially with the applied strain with crossover point around 0.03 % strain for n-Decanol gel and 0.08 % of strain for Propane-1,2-diol gel. Compound A2 in n-Butanol to Proapane-1,2-diol (Figure 4.7) show the same Type- I type of viscoelastic behaviour in all the gel samples.

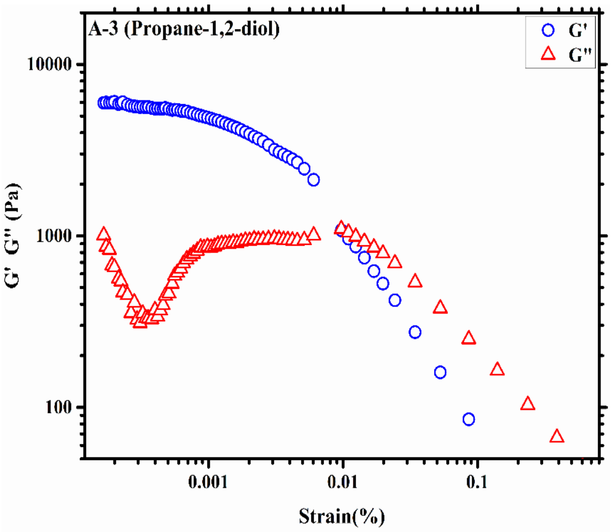


***Figure 4.8*** *Evolution of G’ and G” as a function of oscillation strain of A3 in Propane-1,2-diol.*

Figure 4.8 represents the elastic behaviour of A3 in propane-1,2-diol gel, classified as Type- I with the crossover point of 0.009 % strain. Whereas in case of U1 and U2 in Methanol and Ethanol respectively (fig. 4.8), shows Type III moduli behaviour where G’ decreases and G” increases followed by decrease.

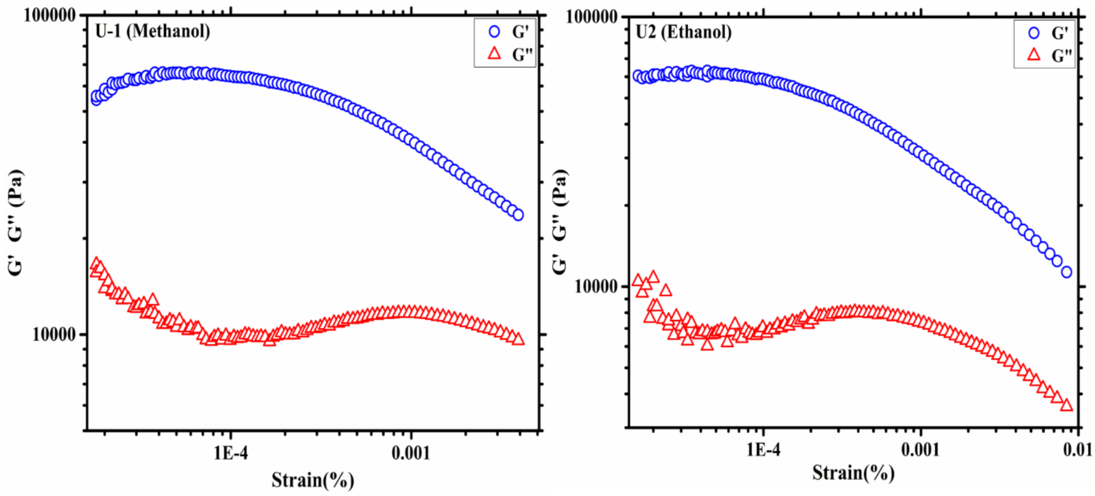


***Figure 4.9*** *Evolution of G’ and G” as a function of oscillation strain of Compound-U1 and U2 in Methanol and Ethanol.*

To compare gelation strength of all the compounds, rheological measurement was carried out in common solvent i.e., Propane-1,2-diol and their data was summarized in the Table 4.3. As evident from the table in all the cases G' is almost three times of G" and the strongest gel was obtained from A2 with the G'/G" ratio of 23.85. the results suggest that A2 has greater stability among all.

***Table 4.3*** *Rheological Parameters extracted from the respective graphs.*

| Compound | Storage modulus(G') (Pa) | Loss modulus(G") (Pa) | G'/G" |
|---|---|---|---|
| A1 | 9161.10 | 3071.24 | 2.98 |
| A2 | 35948.45 | 1507.49 | 23.85 |
| A3 | 5960.16 | 1008.03 | 5.91 |

### 4.4.4 Infrared studies

It is well established that H-bonding and various non-covalent interactions are responsible for supramolecular gelation, therefore Infrared spectroscopy is well known method for the determination of molecular assembly of gelator molecules[38].The solid state FT-IR spectrum of all the compounds show peak around ~3347-3427 $cm^{-1}$ corresponds to N-H stretching[39], band around ~2843-2922 $cm^{-1}$ are from symmetric and anti-symmetric modes of hydrocarbon chains[40].

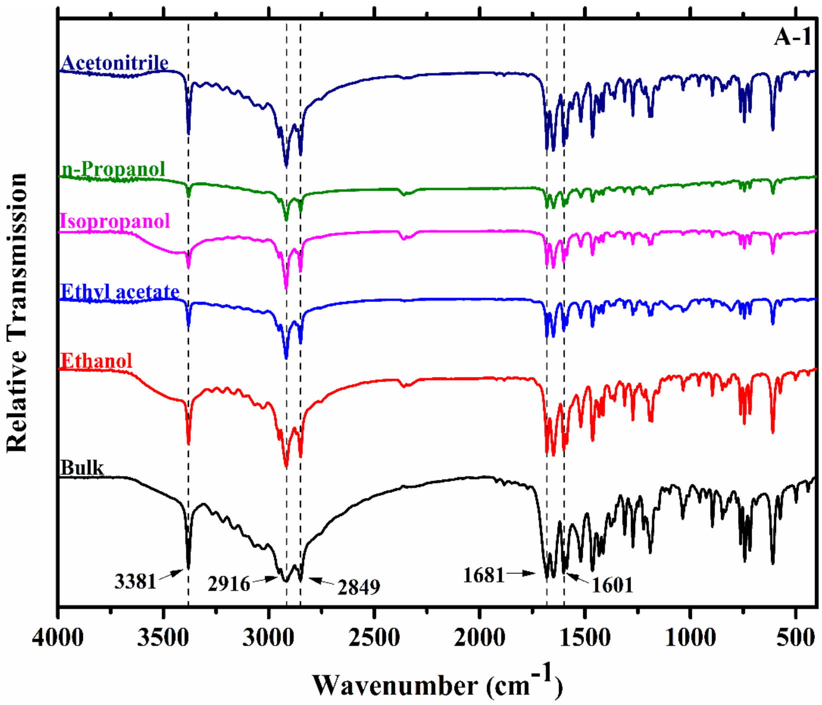


***Figure 4.10*** *IR Spectra of A1 with corresponding xerogels*

Furthermore, peak near ~1681-1719 $cm^{-1}$ correspond to -C=O (amide band I) and C-N (amide II) band appears around ~1463-1471 $cm^{-1}$ [41].

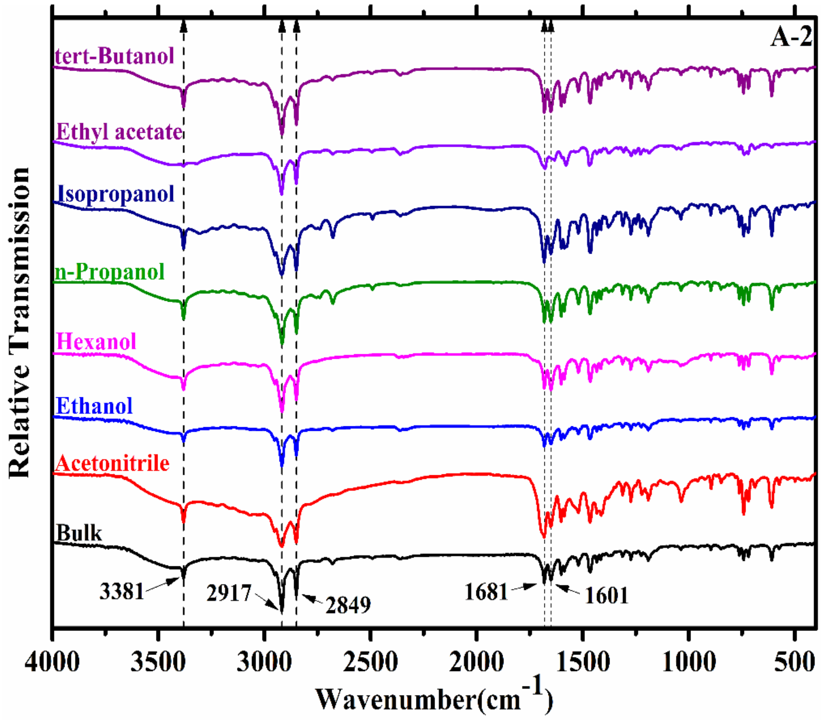


***Figure 4.11*** *IR Spectra of A3 with corresponding xerogels*

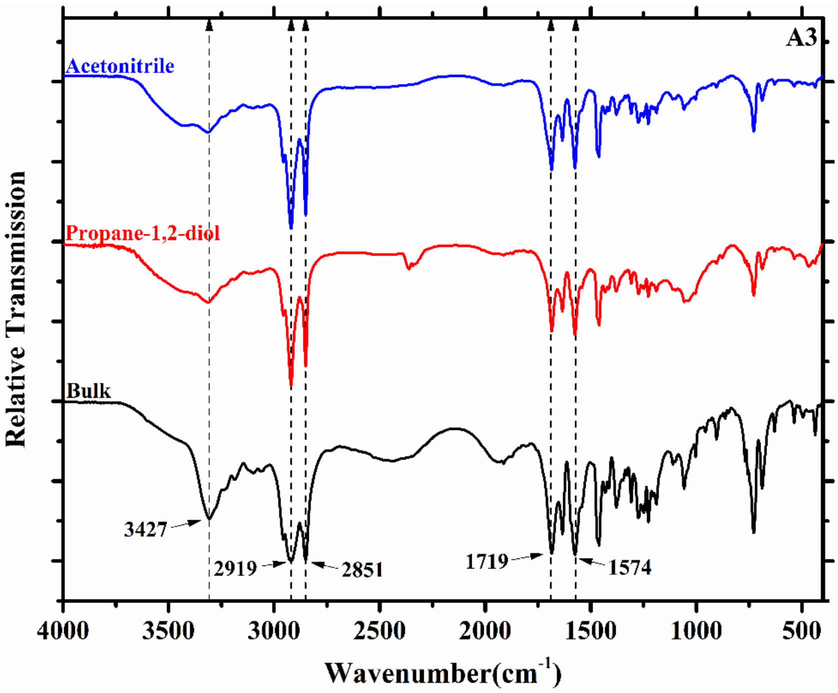


***Figure 4.12*** *IR Spectra of A3 with corresponding xerogels*

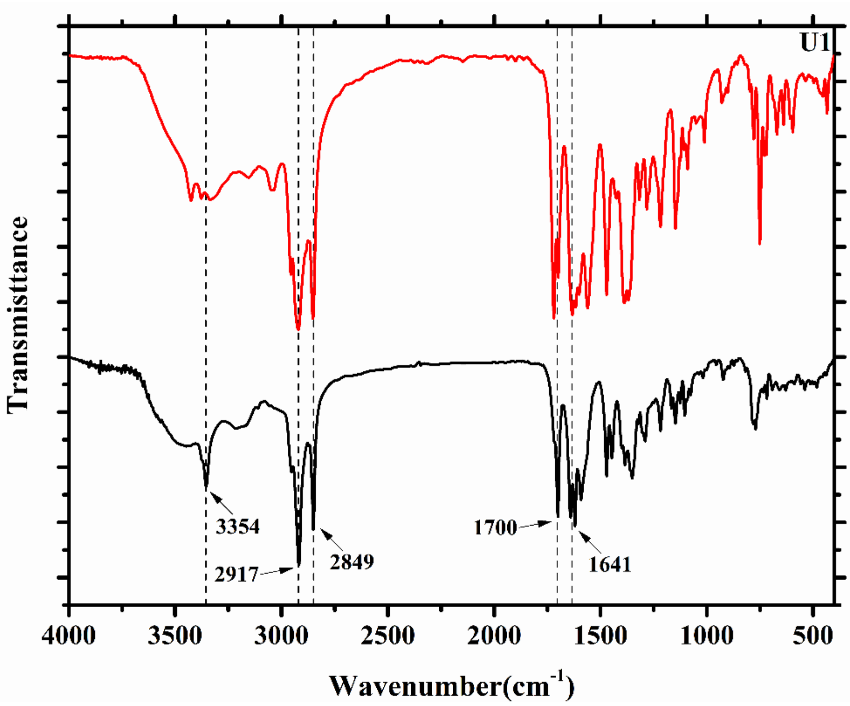


*Figure 4.13 IR Spectra of U1 with corresponding xerogels*

To evaluate role of functional group in the gelation, IR spectrum of all xerogel was obtained from different gel. Surprisingly, almost superimposable spectra of bulk with respective xerogel concludes the retention of non-covalent interactions (Figure 4.10-4.14).

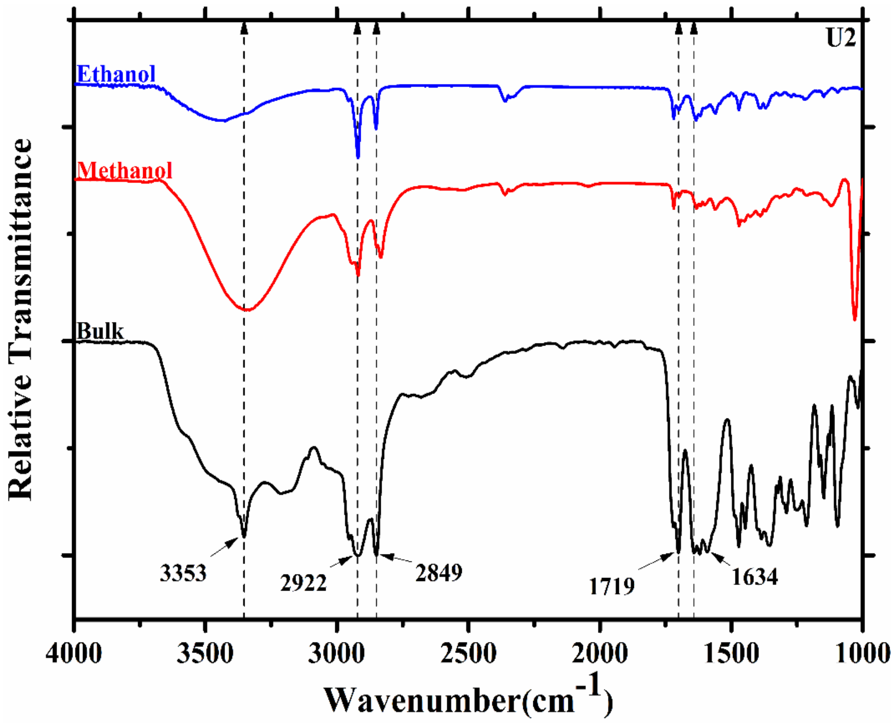


*Figure 4.14 IR Spectra of U2 with corresponding xerogels*

### 4.4.5 Morphological studies

Self-assembly of the gelators molecule creates the 3D network of size from few nanometres to several micrometres which can be easily probed using scanning electron microscope (SEM). Therefore, we measured the morphology of the xerogel obtained from various gel by SEM.

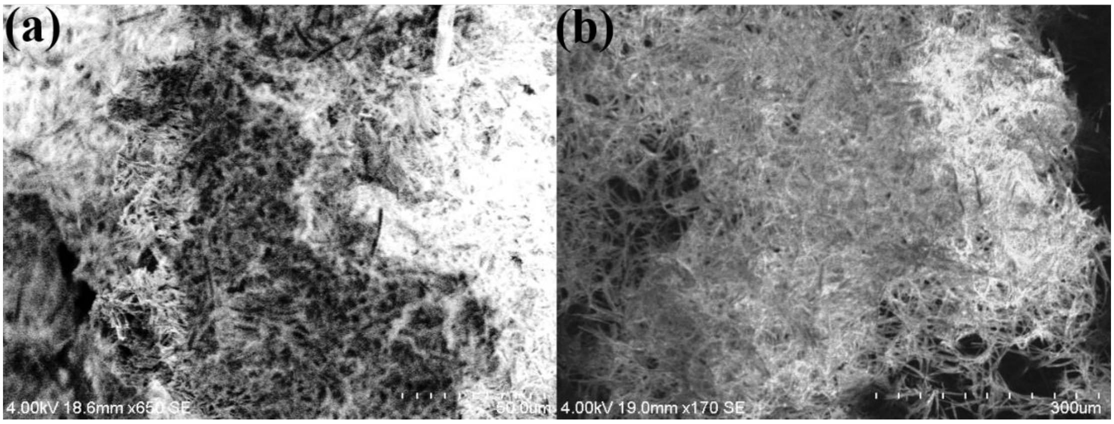


***Figure 4.15*** *SEM micrograph of xerogels of (a) A1 from Ethanol and (b) A-1 from Acetonitrile*

It can be seen that xerogels of A1(Figure 4.15) obtained from Ethanol and acetonitrile shows the fibrous nature having various lengths. In case of xerogel obtained from Ethanol, fibers are less defined and more interconnected as compared to the acetonitrile xerogels where fibers appeared to be linear in nature. Xerogels of A2 and A3(Figure 4.16) (from propane-1,2-diol) appeared to be fibrous 3D network with the high aspect ratio. Additionally, SEM image of gel formed from U1 in methanol showed the fibrous characteristics, whereas the xerogel of U2 obtained from methanol lack fibrous structures (Figure 4.17).

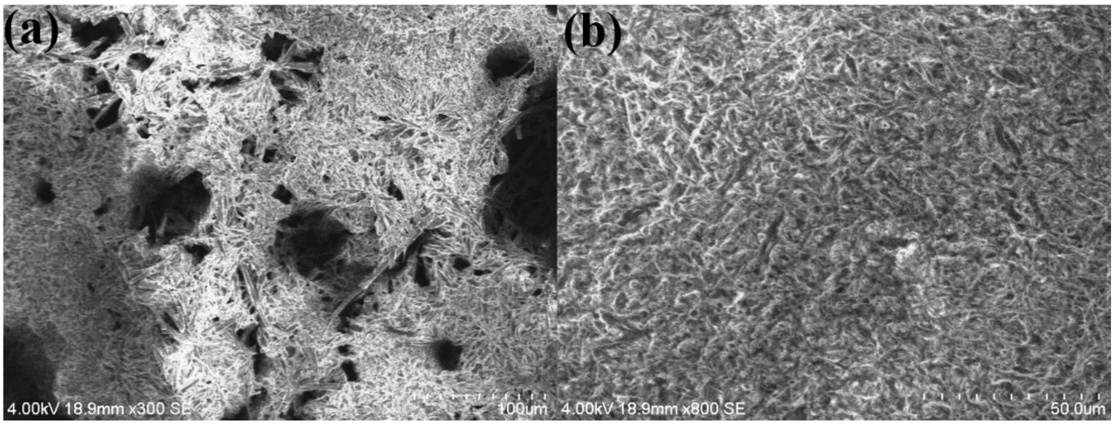


***Figure 4.16*** *SEM micrograph of xerogels of (a) A2 from Acetonitrile and (b) A3 from Prop-1,2-diol*

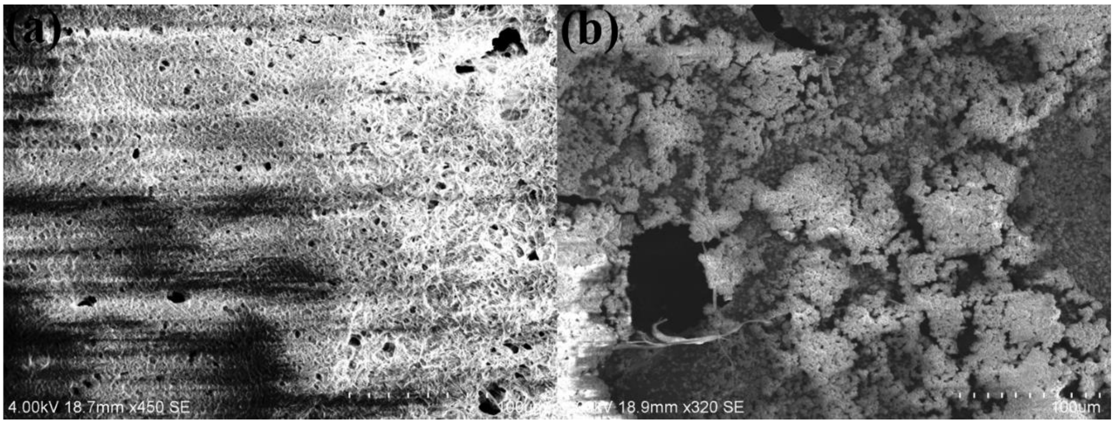


*Figure 4.17 SEM micrograph of xerogels of (a) U1 and (b) U2 from Methanol*

As xerogel morphology structure feature strongly depends on the Gelator-solvent interactions[42], strong gelator-gelators molecule interaction tends to form finer fibrous network, whereas strong solvent-gelator molecule interactions results in the complete loss of fibrous character as seen in the case of U2 xerogel.

### 4.4.6 Powder x-ray diffraction studies

PXRD was consistently used to gain the insight about the packing of gelator molecules in the gel and solid phase[38,43]. Here we compared the diffraction patterns of solid (Bulk) and corresponding xerogels to elaborate the self-assembly process of gelators in various solvent. As expected, diffraction pattern of both bulk and corresponding xerogels are perfectly matching suggested similar packing of molecule in bulk/dried gel. The PXRD spectra of xerogel and bulk of A1 display peaks with the corresponding d-values of 14.74. 7.35, 4.71 and 3.83 for xerogel obtained from acetonitrile (ACN) gel and d-values of 12.95, 6.94, 4.76 and 3.81 for solid(bulk) which are almost following the ratio of 1:1, 1:2, 1:3, and 1:4 suggesting layered structure in both the cases (Figure 4.18).

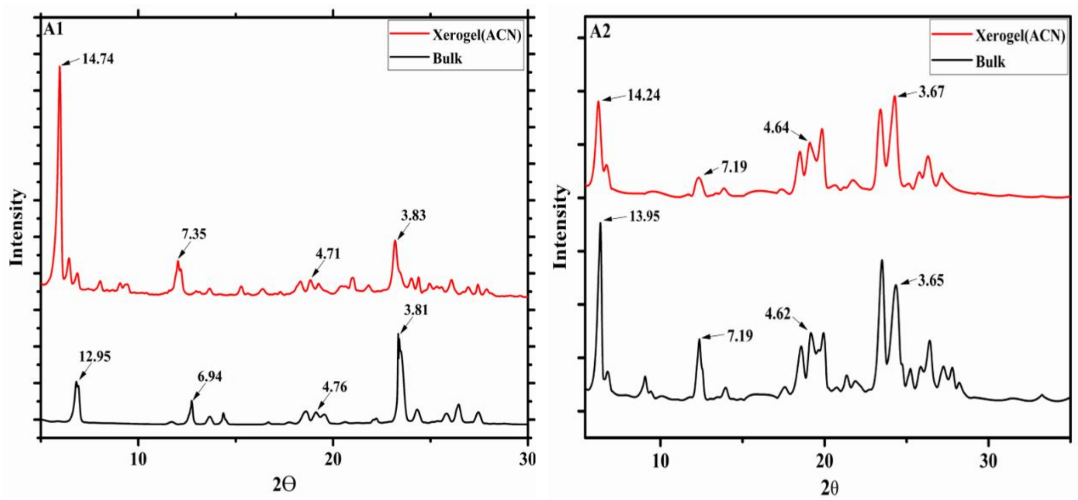


*Figure 4.18 X-ray diffraction pattern of compound A1 and A2 with corresponding xerogels*

Same observations were observed for A2 and A3 xerogels and bulk suggesting layered structure in the both cases (Figure 4.19). It should be noted that, some traces of PXRD signal were observed due the presence of mixed crystal structure of sample.

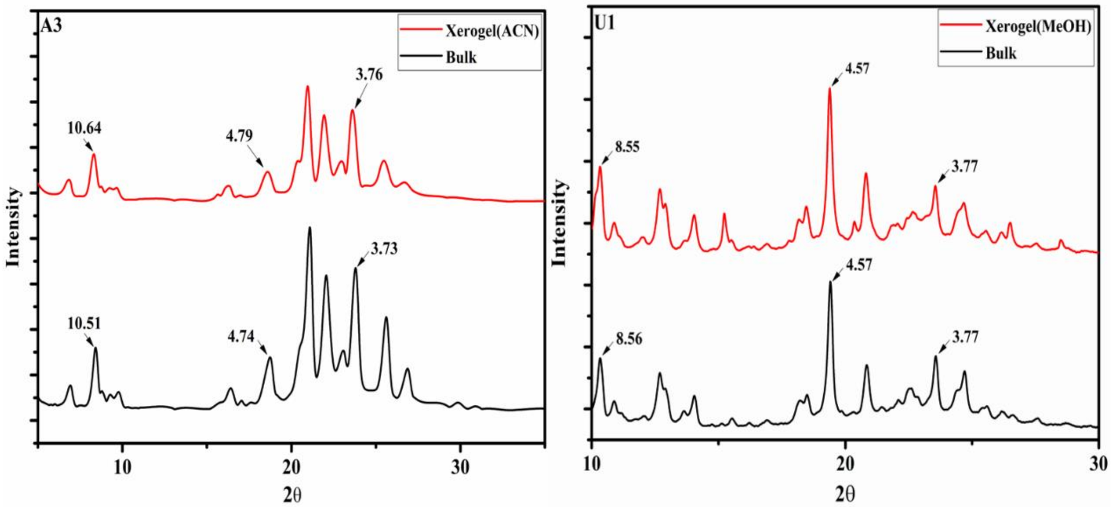


***Figure 4.19*** *X-ray diffraction pattern of compound A3 and U1 with corresponding xerogels*

Additionally, PXRD spectra of U1 and U2 were also carried out, as expected diffraction pattern of bulk and xerogel matches well, implies similar packing. The d-values of three main peaks viz. 8.55, 4.57 and 3.77 follows approximate order of 1:1, 1:2 and 1:3 proposed layered structure. Diffraction profiles of U2 somewhat shows identical behaviour as described above (Figure 4.20).

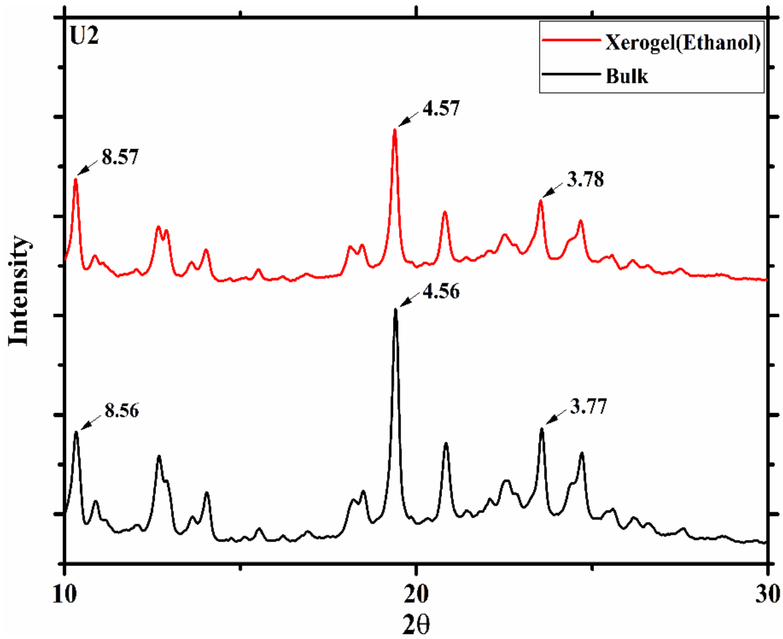


***Figure 4.20*** *X-ray diffraction pattern of compound U2 with corresponding xerogels*

### 4.4.7 Density functional theory studies

It is well known that compounds of urea exhibit both syn-syn and anti-syn conformations[44] and amide containing compounds show syn and anti conformations[45] as shown in scheme 4.4 and 4.5.

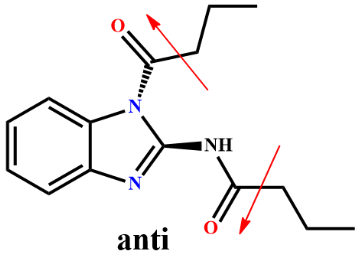


*Scheme 4.4 Schematic of the syn and anti disposition of the amides*

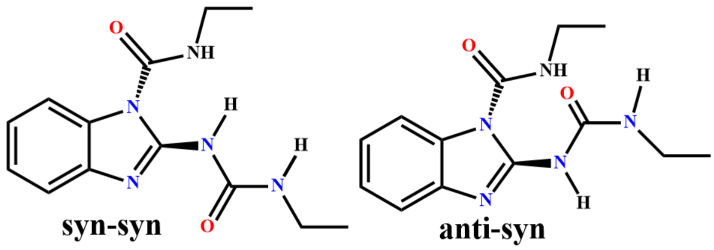


*Scheme 4.5 Schematic of the syn-syn and anti-syn disposition of the urea*

Based on the solvent used for crystallization, specific conformation may preferred in different solvents as different solvents.[46,47] . Despite the multiple crystallization efforts, none of the synthesized compounds formed single crystal suitable of X-ray studies. Therefore, in the absence of crystal structure, we decided to optimized the structure using computational method using B3LYP/6-31(d) basis sets[48] (DFT) to know its conformational preferences.[30,49–51]. The optimized geometry of U2 is shown in Figure 4.21 Where it displayed syn-syn conformation of urea functional group.

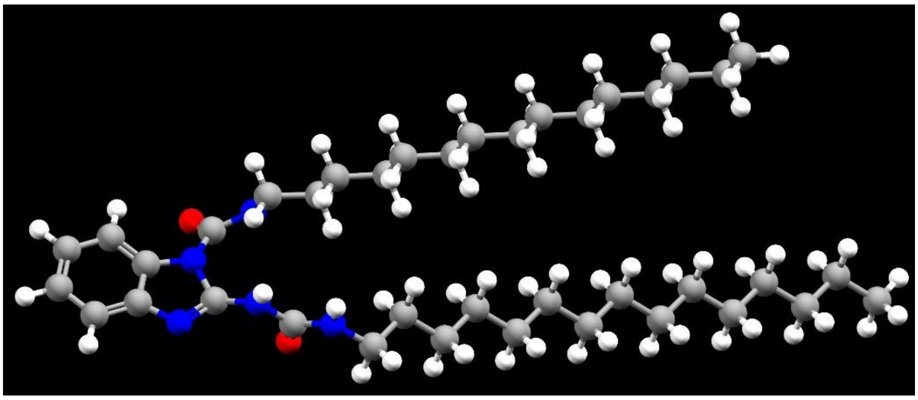

*Figure 4.21: Optimized structure of U2*

As depicted from the structure urea groups are in syn-syn conformer and are rotated out of the plane of the benzimidazole ring and carbonyl groups points in opposite directions (anti parallel). We believed that hydrogen bonds between the oxygen atom of carbonyl group and two N-H atoms forms directional assembly, which was further supported by π- π stacking of benzimidazole units and van der waal interactions of alkyl chain as shown in scheme 4.6.

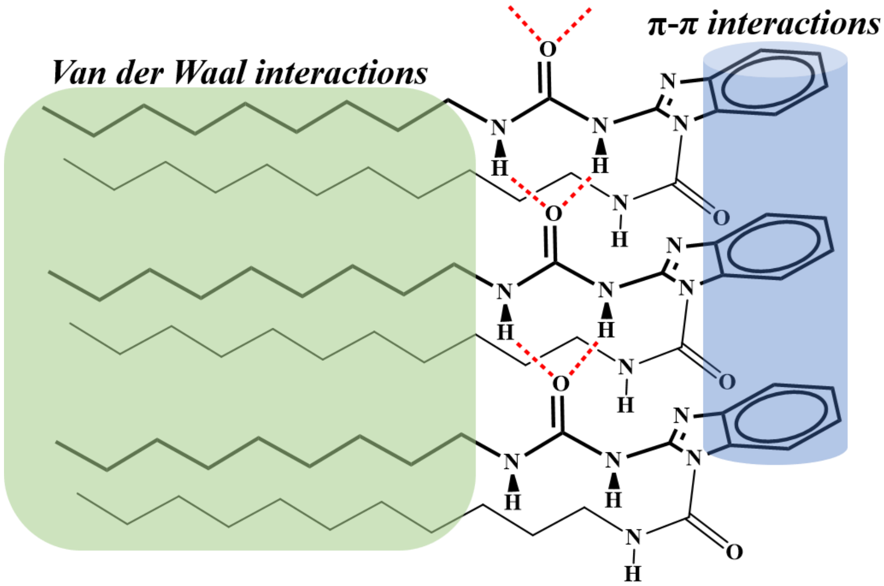


***Scheme 4.6*** *Probable mechanism of bis-Urea compounds*

Furthermore, the optimized geometry of A2 is shown in Figure 4.22, as evident from the structure, A2 preferred anti conformation.

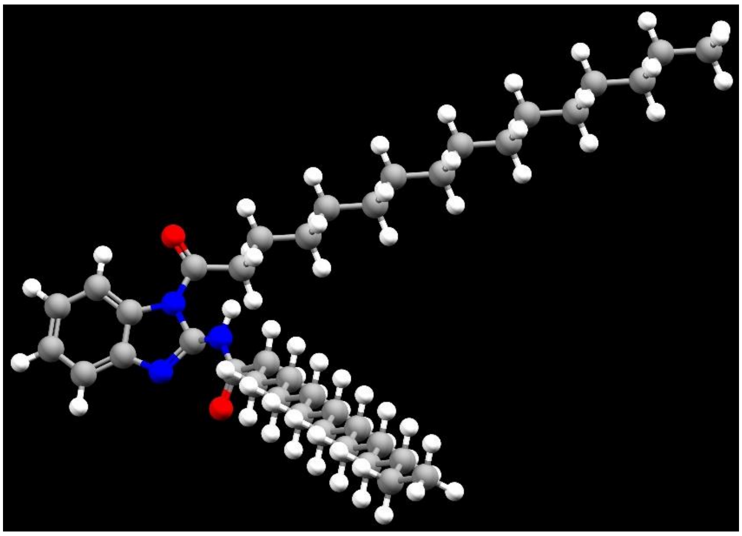

***Figure 4.22*** *Optimized structure of A2*

We proposed that the due to anti conformers, two amides direct itself equatorial to the benzimidazole system and antiparallel to each other which stabilized by two intermolecular N-H···O hydrogen bonding as shown in scheme 4.7 and it is in accordance with the earlier reports[45,52,53].

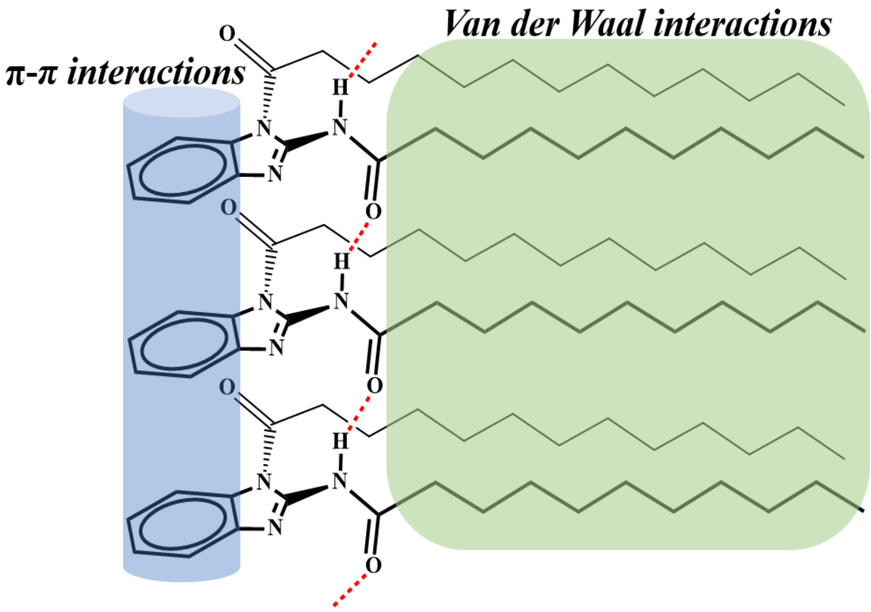


*Scheme 4.7 Probable mechanism of gelation for bisamide*

### 4.4.8 Small angle neutron studies

Small angle neutron scattering(SANS) is fascinating technique of analysis of hydrogels and organogels, provides structural information from few nanometer to micrometer scale[38,43].

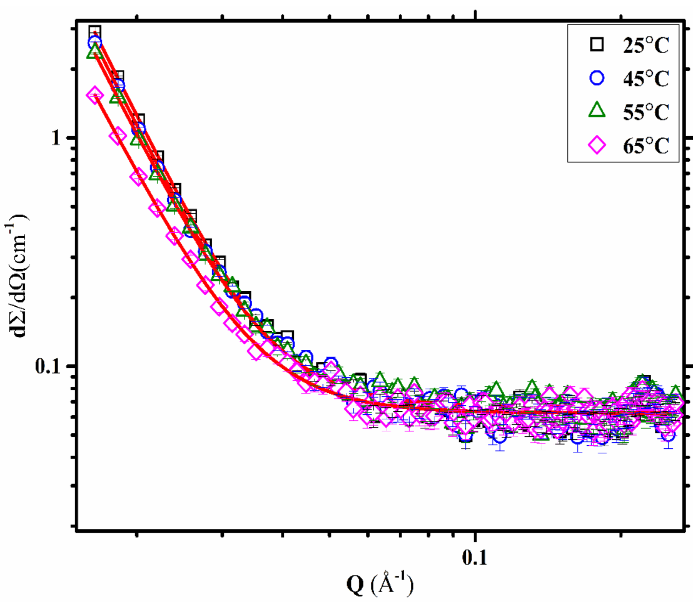


*Figure 4.23 Variable temperature SANS profile of A2 in acetonitrile.*

Here, to probe the structural changes we have collected scattering data for the gels at various temperature obtained from acetonitrile and methanol gel. Due to the Q range used, we unable to fit the data for the specific shape, therefore the data was fitted with traditional two stage network of polymer gels[24,54,55] which is summarized in Table 4.4. Here Figure 4.23 represents the Scattering data of A2 acetonitrile gel at various temperature, as depicted from the plot, initially at 25 °C the correlation length($\xi$) was 165.2 Å with the mass fractal dimension ($D_m$) of 2.50 which changes to $\xi$ =203.3 Å and $D_m$=2.27 at 65 °C.

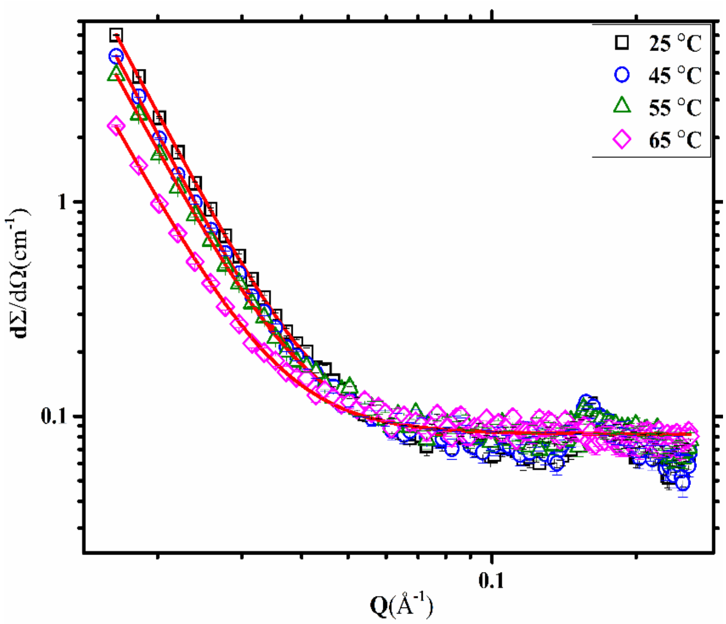


***Figure 4.24*** *Variable temperature SANS profile of A3 in acetonitrile.*

The increase in the correlation length showed the increase in the distance between network, furthermore decrease in the $D_m$ depicts loosening of the gel network. The SANS profile of A3 (Figure 4.24) shows same type of trend, showing $\xi$ =187.8 Å, $D_m$=2.43 at 25 °C temperature with hump around Q=0.1607 $Å^{-1}$ indicating formation of lamellar structure which changes to $\xi$ =276.7 Å, $D_m$=2.20 at 65 °C with subside of hump.

As expected, U1 (Figure 4.25) and U2 (Figure 4.26) also shows identical behaviour, showing change in the $\xi$ from 72.3 Å to 128.1 Å and $D_m$ from 2.77 to 2.29 with increase in the temperature.

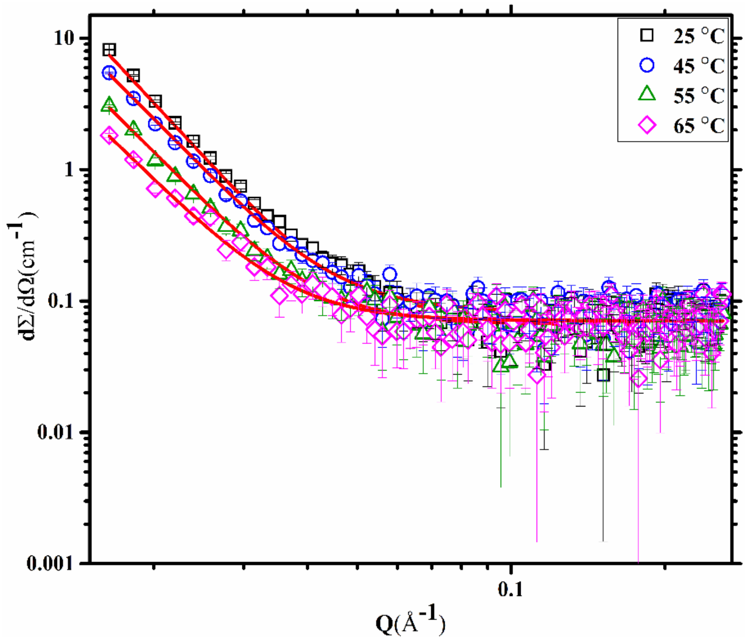


***Figure 4.25*** *Variable temperature SANS profile for U1 in methanol.*

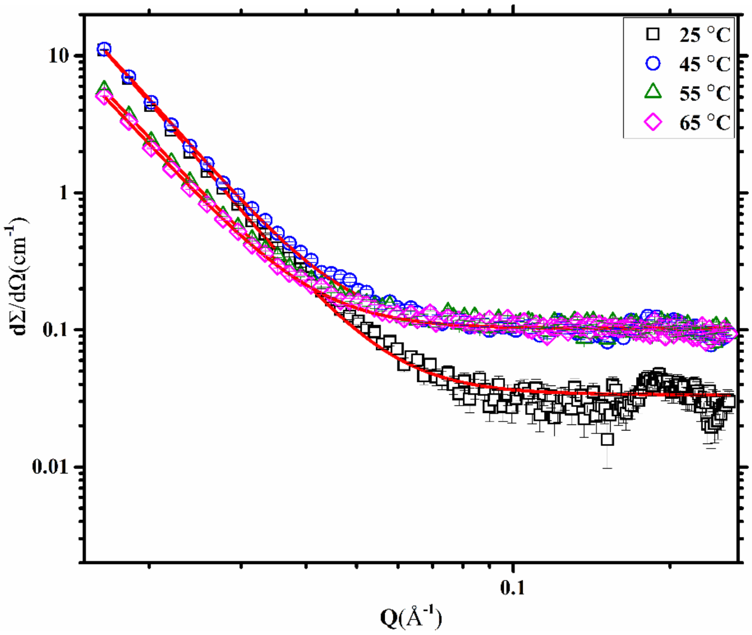


***Figure 4.26*** *Variable temperature SANS profile for U2 in methanol*

*Table 4.4: Dimension data obtained from fitting (Ornstein–Zernike + Mass fractal) of SANS scattering data.*

| System | Temperature (ºC) | Correlation length $\xi$ (Å) | Fractal dimension ($D_m$) |
|---|---|---|---|
| A-2 | 25 | 165.2 | 2.50 |
| | 45 | 173.5 | 2.48 |
| | 55 | 176.8 | 2.41 |
| | 65 | 203.3 | 2.27 |
| A-3 | 25 | 187.8 | 2.43 |
| | 45 | 210.6 | 2.41 |
| | 55 | 218.1 | 2.29 |
| | 65 | 276.7 | 2.20 |
| U-1 | 25 | 72.3 | 2.77 |
| | 45 | 89.0 | 2.60 |
| | 55 | 121.1 | 2.51 |
| | 65 | 128.1 | 2.29 |
| U-2 | 25 | 77.0 | 2.82 |
| | 45 | 78.3 | 2.72 |
| | 55 | 108.5 | 2.47 |
| | 65 | 115.1 | 2.46 |

### 4.4.9 Sensing Studies

As we know that heterocyclic scaffold is one of the most preferred structural entities to detect various analytes in the solution. Among all structural units, benzimidazole is a first choice to create the sensor with the diverse applications as a chemosensor[17].Despite of various reports, field of supramolecular gel consist of benzimidazole unit which can be used to detect the analytes are still growing[19,20].

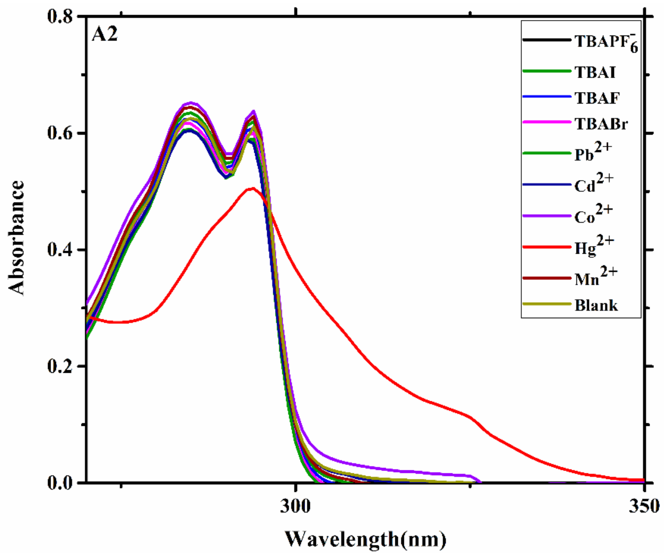


***Figure 4.27** Changes in the UV-Vis spectrum of A2(50 μM) upon addition of 6 equivalents of cations and anions.*

Therefore, presence of Urea and amide in our system prompted us to study stimuli responsive nature of A2 and B2. Here, to begin with anion sensing capability of anions like Iodide ($I^-$), fluoride ($F^-$), Bromide ($Br^-$), and Hexafluorophosphate ($PF_6^-$) was checked by adding 2 equivalents of their tetrabutylammonium salts as shown in the figure 4.27 and afterward various metals like Lead ($Pb^{2+}$), Cadmium ($Cd^{2+}$), Cobalt ($Co^{2+}$), Mercury ($Hg^{2+}$) and Manganese ($Mn^{2+}$), acetate as counter anions salts were examined.

Interestingly, no anion/cations were able to show any significant change in the $\lambda_{max}$ value except $Hg^{2+}$ ion. The formation of $Hg^{2+}$-A2 Complex resulted in the appearance of a new peak.

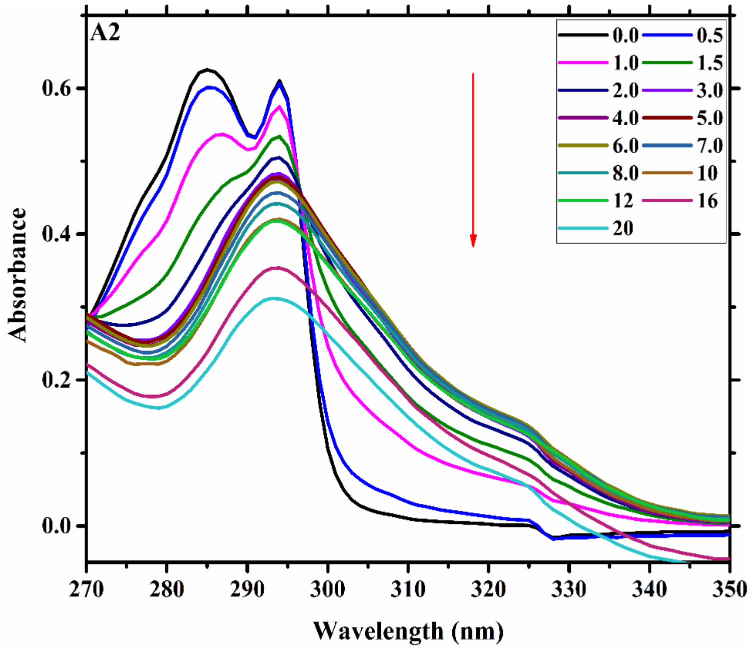


***Figure 4.28*** *UV spectra of A2(50 μM) with various concentration $Hg^{2+}$*

In the absorption spectra receptor A2 showed band near 285 nm and sharp band at 294 nm. After addition of 2 equivalents of $Hg^{2+}$, the intensity of band near 285 nm was found to be diminished and band near 294 nm was unchanged. Interaction between A2 and $Hg^{2+}$ was studied further by spectrophotometric titration experiments (Fig 4.28) and found that band near 285 nm and 294 nm decreased gradually, then band around 285 nm was vanished at high concentration of $Hg^{2+}$.

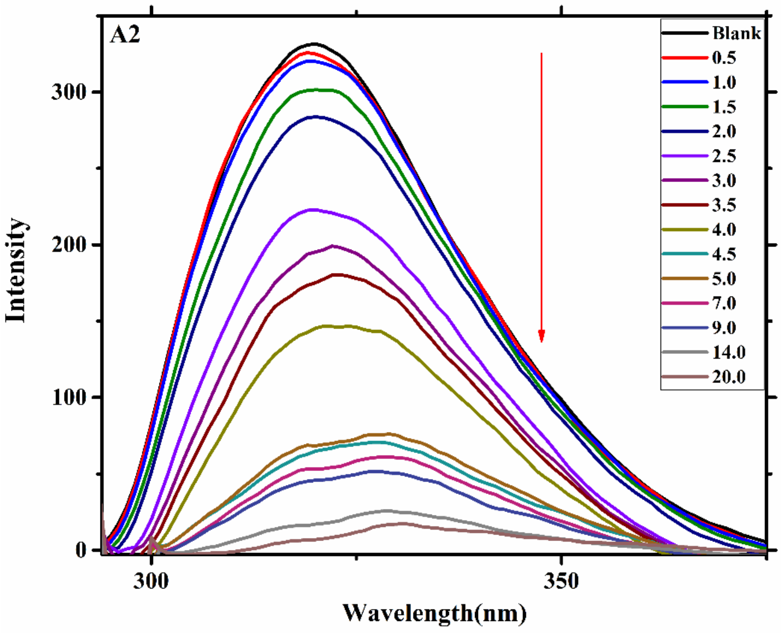


***Figure 4.29*** *Change in emission spectra A2(50 μM) with the gradual increase in the concentration of $Hg^{2+}$*

Figure 4.29 shows the fluorescence spectra of A2 with emission at 320 nm when excited at 285 nm. Stepwise addition of $Hg^{2+}$ solution was found to clearly quench the emission peak supporting the formation of $Hg^{2+}$-A2 complex.

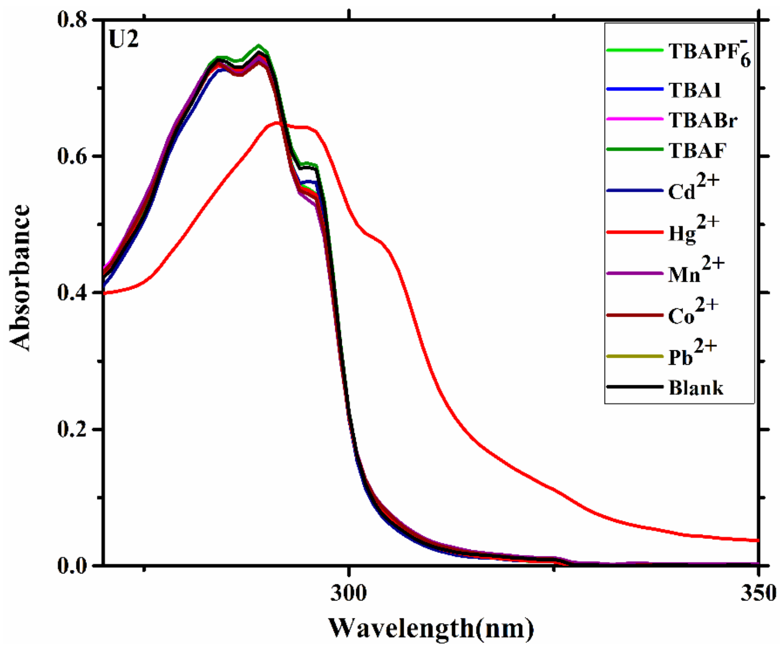


***Figure 4.30*** *Changes in the UV-Vis spectrum of U2 upon addition of 6 equivalents of cations and anions*

The jobs plot was plotted and stoichiometry was found to be 1:2($Hg^{2+}$-A2) with limit of detection (LOD) of 8.9 x $10^{-3}$ **μ**M. Similarly, the absorption spectra of B2 (figure 4.30) shows absorption maxima at 284 nm, 289 nm and 295 nm. After titration with 6 equivalents of different anions and metal ions, B2 showed the formation of new peak only in the case of $Hg^{2+}$ ion. It may be interpreted that the formation of $Hg^{2+}$-B2 complex leads to the appearance of new absorption band with the absorption maxima at 290, 295 and 303 nm (figure 4.31).

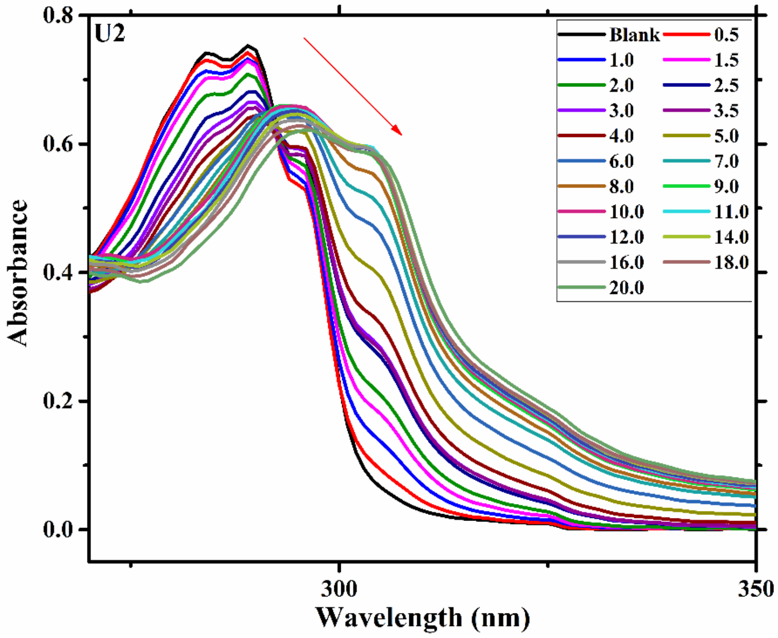


***Figure 4.31**: UV spectra of U2 with various concentration $Hg^{2+}$*

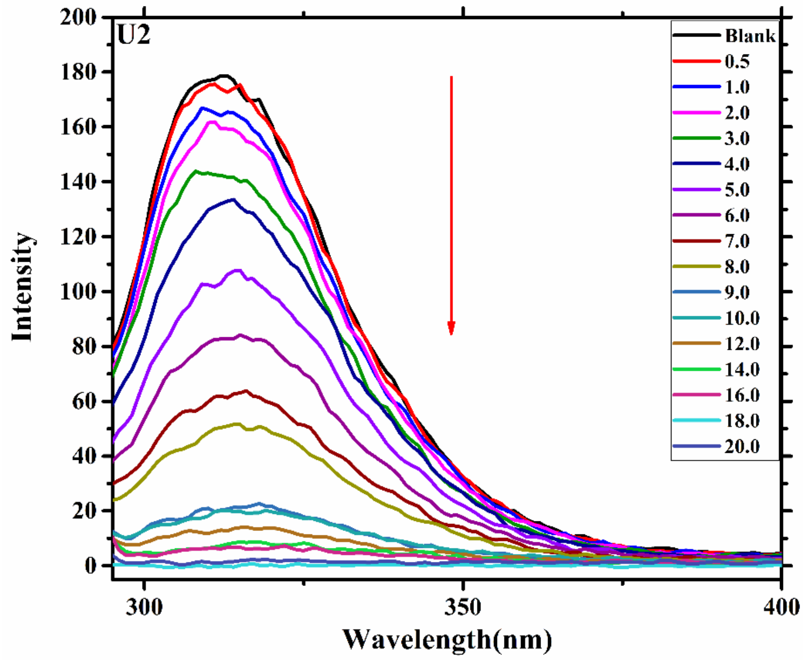


***Figure 4.32** Change in emission spectra B2 in THF (50 μM) upon gradual addition of $Hg^{2+}$; excitation wavelength 285 nm.*

Florescence spectra of B2 (figure 4.32) shows emission at 314 nm when excited at 285 nm, the step wise addition of $Hg^{2+}$(upto 20 equivalents) displayed the decrease in the band at 314 nm. In this case also Job's plot was used to determine the composition of $Hg^{2+}$: B2 complex and found to be 1:1 and LOD calculated was 1.16 x $10^{-3}$ **μ**M.

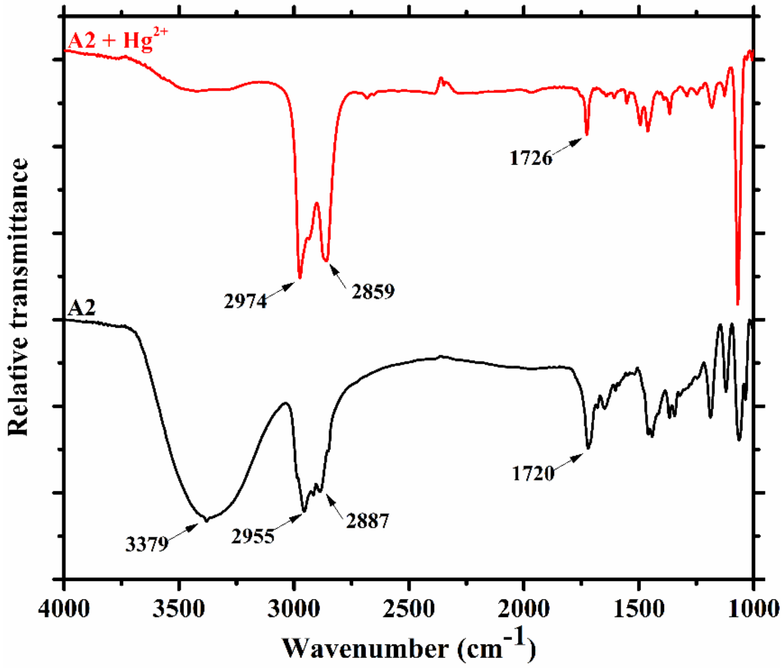


***Figure 4.33*** *IR spectra of A2 in THF before and after addition of $Hg^{2+}$*

Additionally, we investigated the impact of high concentration of mercury on the gel of compound A2 and U2 in ethanol solvent by adding powdered mercury acetate (2 equivalent) on the upper layer of gel, no degelation or breaking of gel was observed suggesting the retention of supramolecular assembly even in the presence of mercury ions. To explore the binding mode of A2 and B2 with the $Hg^{2+}$, $^{1}H$ NMR spectra was recorded in the presence of 0.5 to 2.0 equivalents of $Hg^{2+}$ in $CDCL_3$. It is found that addition of mercury broadens the signal in aromatic region, furthermore, NH signals are not visible due the rapid exchange of N-H protons with solvent. FT-IR was additionally done to probe the interactions between our receptors and $Hg^{2+}$. A2 shows peaks for N-H at 3379 $cm^{-1}$, 2955-2887 $cm^{-1}$ for $CH_2$ symmetric and asymmetric vibration(fig. 4.33), 1720 $cm^{-1}$ for carbonyl(-C=O) stretching in THF solution which was compared with absorption peak of A2 + $Hg^{2+}$ in the solution phase, N-H peak was completely disappeared, at same moment peak of $CH_2$ and carbonyl shifted to 2974-2859 $cm^{-1}$ and 1726 $cm^{-1}$, which demonstrate the involvement of N-H, moreover shift of $CH_2$ and C=O refers to the weakening of intermolecular hydrogen bonding.

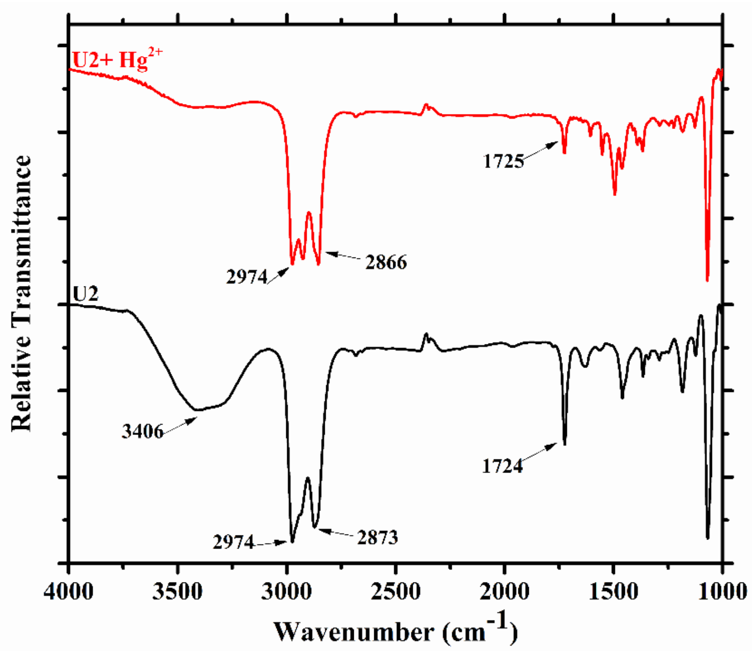


***Figure 4.34*** *IR spectra of U2 in THF before and after addition of $Hg^{2+}$*

Similarly, IR spectra of U2 shows N-H peak at 3406 $cm^{-1}$ and peak at 2974- 2873 $cm^{-1}$ corresponds to $CH_2$ symmetric and asymmetric stretching vibrations, peak at 1724 $cm^{-1}$ is due to -C=O stretching vibrations. Interesting, addition of $Hg^{2+}$ to the U2 solution leads to disappearance of N-H peak, but no change was observed for remaining peaks (figure 4.34).

## 4.5 Conclusions

In the present study, a new class of benzimidazole based bisamide and bisurea supramolecular gelators are reported. The two series of gelators under investigation share structural similarities, but the intermolecular interactions that cause gelation differ systematically depending on the length of the alkyl tail and the quantity of hydrogen bonding units that are present. The gelation properties in different solvents and mixture of solvents were carried out, and their thermal stability, thermoreversiblity was checked. Bisamide compound (A1, A2 and A3) exhibited excellent gelation capability in polar solvents (specially alcohols) whereas Bisurea compounds (U1, U2 and U3) unable to gelate most of the solvents, used in the present study. Solvent parameter studies revealed that the gelation properties were dependent on refractive index of solvent, polarizability and dispersion interactions. Particularly presence of extra N-H group doesn't improve gelation properties, but to our understanding it strengthens the intermolecular H-bonding which makes the molecule to precipitate out rapidly from the solvent instead of fibre formation. Amide derivatives whereas has improved balance between crystallization and solvation due to the combine effect of both Hydrogen bonding, van der Waals interaction. PXRD studies of Bulk and gelator concludes the similar packing in bulk and xerogel state with the presence of layered structure. The temperature variation SANS study was employed to probed the gelation morphology and concluded that shape independent morphology in gel state which is further supported by the SEM images. Furthermore, A2 and B2 are explored for their capability as a chemosensor for detection of different anions such as $I^-$, $F^-$, $Br^-$, and $PF_6^-$, $Pb^{2+}$, $Cd^{2+}$, $Co^{2+}$, $Hg^{2+}$ and $Mn^{2+}$ found to interact only with $Hg^{2+}$ confirms by UV-Visible and Fluorescence spectroscopy with very low LOD.

## References


1. Gale, P. A. & Caltagirone, C. Anion sensing by small molecules and molecular ensembles. *Chem. Soc. Rev.* **44**, 4212–4227 (2015).
2. Picci, G. *et al.* Anion-Responsive Fluorescent Supramolecular Gels. *Molecules* **27**, 1257 (2022).
3. Yang, X., Zhang, G. & Zhang, D. Stimuli responsive gels based on low molecular weight gelators. *J. Mater. Chem.* **22**, 38–50 (2012).
4. Piepenbrock, M. M., Lloyd, G. O., Clarke, N. & Steed, J. W. Metal- and Anion-Binding Supramolecular Gels. *Chem. Rev.* **110**, 1960–2004 (2010).
5. Okesola, B. O. & Smith, D. K. Applying low-molecular weight supramolecular gelators in an environmental setting-self-assembled gels as smart materials for pollutant removal. *Chem. Soc. Rev.* **45**, 4226–4251 (2016).
6. Fang, W. *et al.* Recent Advances in Supramolecular Gels and Catalysis. *Chemistry - An Asian Journal* **13**, 712–729 (2018).
7. Skilling, K. J. *et al.* Insights into low molecular mass organic gelators: A focus on drug delivery and tissue engineering applications. *Soft Matter* **10**, 237–256 (2014).
8. Christoff-Tempesta, T., Lew, A. J. & Ortony, J. H. Beyond covalent crosslinks: Applications of supramolecular gels. *Gels* **4**, (2018).
9. Terech, P. & Weiss, R. G. Low molecular mass gelators of organic liquids and the properties of their gels. *Chem. Rev.* **97**, 3133–3159 (1997).
10. Yamanaka, M. Urea derivatives as low-molecular-weight gelators. *J. Incl. Phenom. Macrocycl. Chem.* **77**, 33–48 (2013).
11. Sivakova, S. & Rowan, S. J. Nucleobases as supramolecular motifs. *Chem. Soc. Rev.* **34**, 9–21 (2005).
12. Tomasini, C. & Castellucci, N. Peptides and peptidomimetics that behave as low molecular weight gelators. *Chem. Soc. Rev.* **42**, 156–172 (2013).
13. Smith, D. K. Dendritic supermolecules - Towards controllable nanomaterials. *Chem. Commun.* 34–44 (2006).
14. Dydio, P., Lichosyt, D. & Jurczak, J. Amide- and urea-functionalized pyrroles and benzopyrroles as synthetic, neutral anion receptors. *Chem. Soc. Rev.* **40**, 2971–2985 (2011).
15. Patel, A. & Ballabh, A. Design , Synthesis and Applications of Urea derivatives as low- molecular-weight gelators. **390002**, 390002
16. Panja, S. & Ghosh, K. Progress in Benzimidazole/Benzimidazolium-Derived Supramolecular Gelators in Ion Recognition. *Mini. Rev. Org. Chem.* **17**, 1042–1055 (2020).
17. Horak, E., Kassal, P. & Murković Steinberg, I. Benzimidazole as a structural unit in fluorescent chemical sensors: the hidden properties of a multifunctional heterocyclic scaffold. *Supramol. Chem.* **30**, 838–857 (2018).
18. Molina, P., Tárraga, A. & Otón, F. Imidazole derivatives: A comprehensive survey of their recognition properties. *Org. Biomol. Chem.* **10**, 1711–1724 (2012).
19. Panja, S. & Ghosh, K. Progress in Benzimidazole/Benzimidazolium-Derived Supramolecular Gelators in Ion Recognition. *Mini. Rev. Org. Chem.* **17**, 1042–1055 (2020).
20. Beloqui, A. Supramolecular Assembly of Benzimidazole Derivatives and Applications. *Chem. Appl. Benzimidazole its Deriv.* 1–13 (2019).

doi:10.5772/intechopen.85333

21. Zweep, N. *et al.* Balancing hydrogen bonding and van der waals interactions in cyclohexane-based bisamide and bisurea organogelators. *Langmuir* **25**, 8802–8809 (2009).
22. Aswal, V. K. & Goyal, P. S. Small-angle neutron scattering diffractometer at Dhruva reactor. *Curr. Sci.* **79**, 947–953 (2000).
23. Takata, S. I., Norisuye, T. & Shibayama, M. Small-angle neutron-scattering study on preparation temperature dependence of thermosensitive gels. *Macromolecules* **35**, 4779–4784 (2002).
24. Shibayama, M. Small-angle neutron scattering on polymer gels: Phase behavior, inhomogeneities and deformation mechanisms. *Polym. J.* **43**, 18–34 (2011).
25. Saffer, E. M. *et al.* SANS study of highly resilient poly(ethylene glycol) hydrogels. *Soft Matter* **10**, 1905 (2014).
26. Chen, S. H. & Teixeira, J. Structure and fractal dimension of protein-detergent complexes. *Phys. Rev. Lett.* **57**, 2583–2586 (1986).
27. Teixeira, J. Small-angle scattering by fractal systems. *J. Appl. Crystallogr.* **21**, 781–785 (1988).
28. Luo, X., Li, Z., Xiao, W., Wang, Q. & Zhong, J. Self-assembled organogels formed by monochain derivatives of ethylenediamine. *J. Colloid Interface Sci.* **336**, 803–807 (2009).
29. Patel, A. M., Ray, D., Aswal, V. K. & Ballabh, A. Probing the mechanism of gelation and anion sensing capability of a thiazole based amide gelator: A case study. *Colloids Surfaces A Physicochem. Eng. Asp.* **607**, 125430 (2020).
30. Patel, A. M., Ray, D., Aswal, V. K. & Ballabh, A. Probing the supramolecular assembly in solid , solution and gel phase in uriede based thiazole derivatives and its potential application as iodide ion sensor. *J. Mol. Liq.* **362**, 119763 (2022).
31. Lan, Y., Corradini, M. G., Weiss, R. G., Raghavan, S. R. & Rogers, M. A. To gel or not to gel: correlating molecular gelation with solvent parameters. *Chem. Soc. Rev.* **44**, 6035–6058 (2015).
32. Hildebrand, J. H. & Scott, R. L. *The Solubility of Nonelectrolytes*. (Dover Publications, Reinhold, NY, 1959).
33. Hansen, C. M. The Three Dimensional Solubility Parameter - Key to Paint Component Affinities I. - Solvents, Plasticizers, Polymers, and Resins. *J. Paint Techn* 104–117 (1967).
34. Lan, Y. et al. Comparing and correlating solubility parameters governing the selfassembly of molecular gels using 1,3:2,4-dibenzylidene sorbitol as the gelator. *Langmuir* **30**, 14128–14142 (2014).
35. Barton, A. F. M. Solubility Parameters. *Chem. Rev.* **75**, 731–753 (1975).
36. Mezger, T. G. *The Rheology Handbook: For Users of Rotational and Oscillatory Rheometers*. (Vincentz Network GmbH & Co. KG: Hannover, 2006).
37. Sim, H. G., Ahn, K. H. & Lee, S. J. Large amplitude oscillatory shear behavior of complex fluids investigated by a network model: A guideline for classification. *J. Nonnewton. Fluid Mech.* **112**, 237–250 (2003).
38. Yu, G., Yan, X., Han, C. & Huang, F. Characterization of supramolecular gels. *Chem. Soc. Rev.* **42**, 6697–6722 (2013).
39. Mido, Y. An infrared study of various dialkylureas in solution. *Spectrochim. Acta Part A* **29A**, 431–438 (1973).
40. Higashi, A., Czarnecki, M. A. & Ozaki, Y. Infrared study of solids and cast films of long-chain fatty acids. *Thin Solid Films* **230**, 203–208 (1993).

41. Pierce, A. M., Maslanka, P. J., Carr, A. J. & Mccain, K. S. Using fourier transform Infrared spectroscopy to examine structure in bisurea organogels. *Appl. Spectrosc.* **61**, 379–387 (2007).
42. Zhu, G. *et al.* Solvent Effect on Organogel Formation by Low Molecular Weight Molecules. *Chem. Eur. J.* **19**, 9234–9241 (2013).
43. Denzer, B. R., Kulchar, R. J., Huang, R. B. & Patterson, J. Advanced methods for the characterization of supramolecular hydrogels. *Gels* **7**, 158 (2021).
44. Phukan, N. & Baruah, J. B. Conformational adjustments over synthons of urea and thiourea based assemblies. *CrystEngComm* **18**, 7753–7763 (2016).
45. Pi-boleda, B., Sans, M., Nolis, P. & Illa, O. Studies on Cycloalkane-Based Bisamide Organogelators : A New Example of Stochastic Chiral Symmetry-Breaking Induced by Sonication. *Chem. Eur. J.* **23**, 3357–3365 (2017).
46. Cox, C. & Lectka, T. Solvent Effects on the Barrier to Rotation in Carbamates Table 1. Solvent Effects on the Barrier to Rotation of Amide 1 and Carbamate 2 a. *J. Org. Chem.* **63**, 2426–2427 (1998).
47. Rablen, P. R. *et al.* Solvent Effects on the Barrier to C−N Bond Rotation in N,N-Dimethylaminoacrylonitrile: Modeling by Reaction Field Theory and by Monte Carlo Simulations. *J. AM. CHEM. SOC* **121**, 218–226 (1999).
48. Robert G. Parr, W. Y. Density-Functional Theory of the Electronic. *Annu. Rev. Phys. Chem.* **46**, 701–728 (1995).
49. Smith, A. E. The crystal structure of the urea–hydrocarbon complexes. *Acta Crystallogr.* **5**, 224–235 (1952).
50. Harris, K. D. M. & Thomas, J. M. Structural aspects of urea inclusion compounds and their investigation by X-ray diffraction: A general discussion. *J. Chem. Soc. Faraday Trans.* **86**, 2985–2996 (1990).
51. Vlatkovic, M., Feringa, B. L. & Wezenberg, S. J. Dynamic inversion of stereoselective phosphate binding to a bisurea receptor controlled by light and heat. *Angew. Chemie - Int. Ed.* **55**, 1001–1004 (2016).
52. Prominent Gelation and Chiral Aggregation of Alkylamides Derived from trans-1,2-Diaminocyclohexane. *Communications* **35**, 1949–1951 (1996).
53. David Dıaz Dıaz, Tomas Torres, Rudolf Zentel, b R. D. and M. B. Physicochemical characterization of octakis ( alkyloxy ) -substituted Zn ( II ) -phthalocyanines non-covalently incorporated into an organogel and their remarkable morphological effect on the nanoscale-fibers. *Chem. Commun.* 2369–2371 (2007).
54. Shibayama, M. Structure-mechanical property relationship of tough hydrogels. *Soft Matter* **8**, 8030–8038 (2012).
55. Yang, Z. *et al.* Nonlinear Behavior of Gelatin Networks Reveals a Hierarchical Structure. *Biomacromolecules* **17**, 590–600 (2016).

# Supporting information

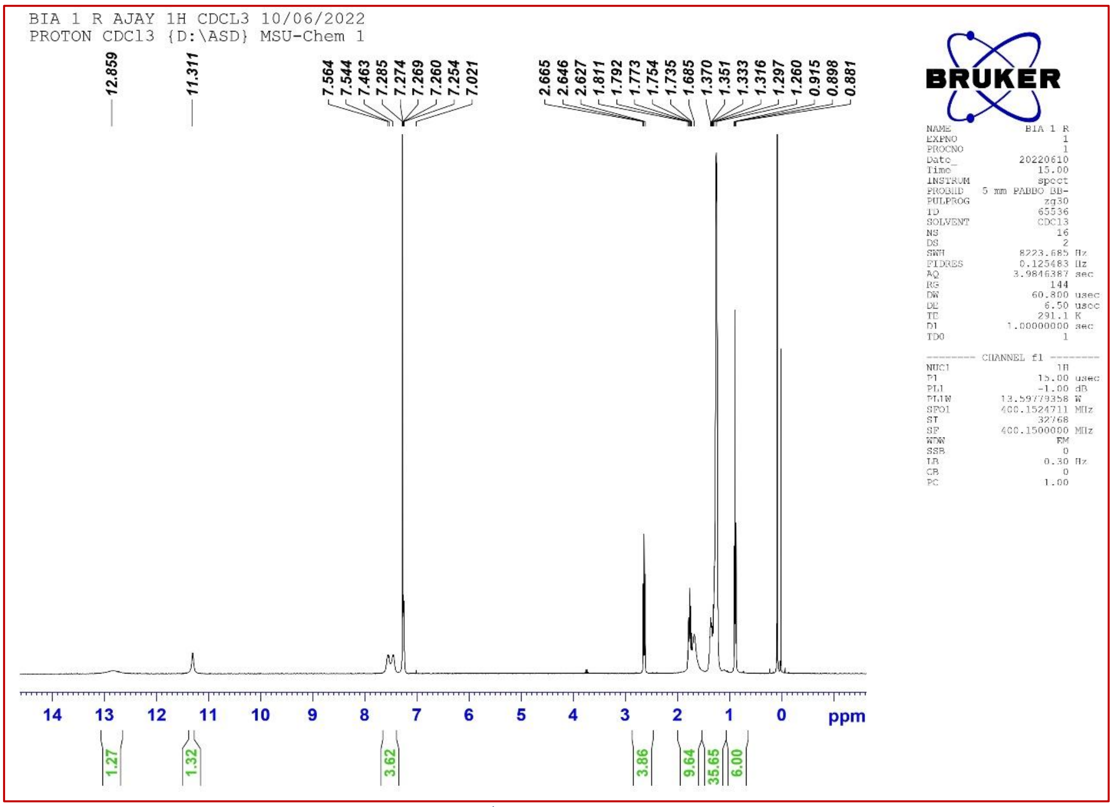

*Figure 35* $^{1}$*H NMR spectra of A1*

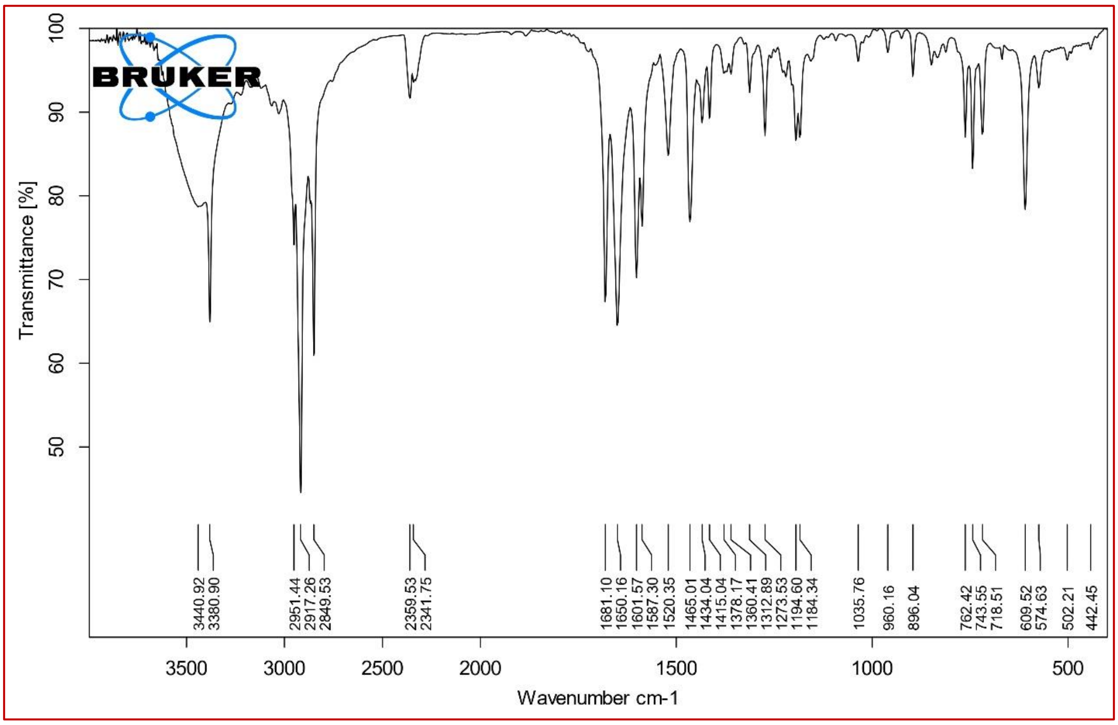

*Figure 36 IR spectra of A1*

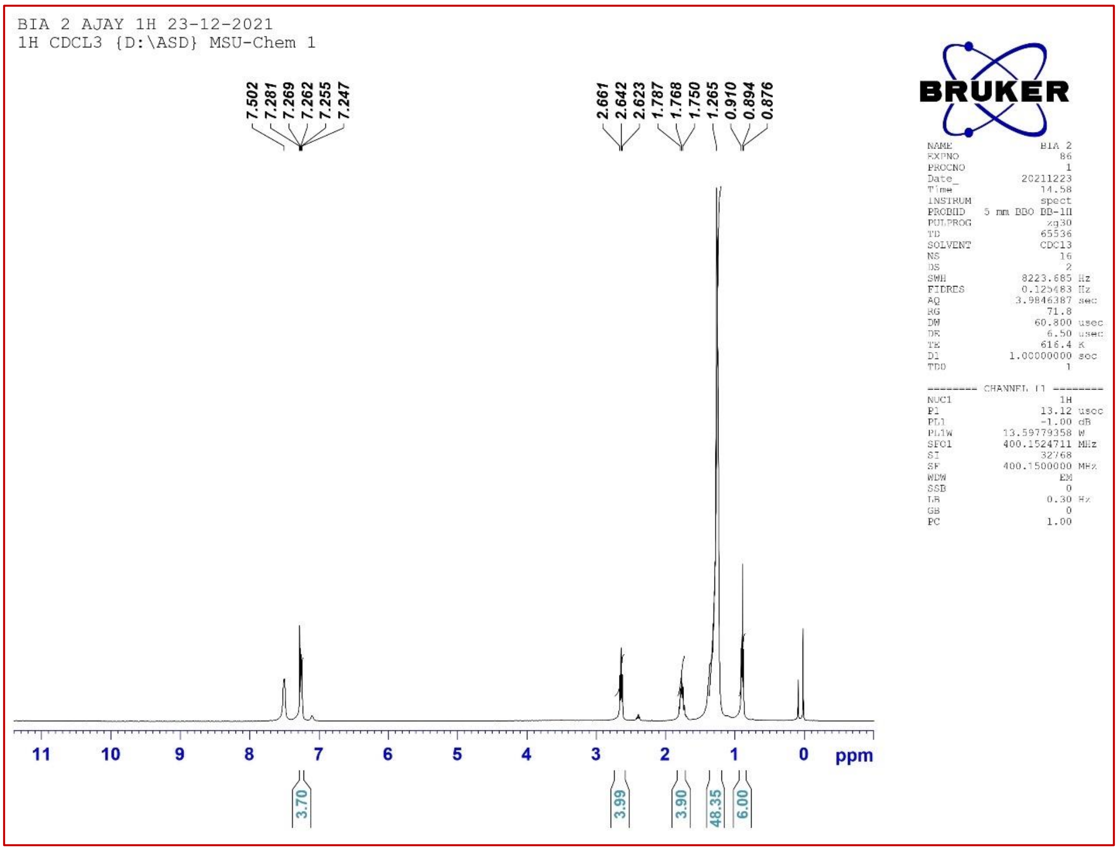


***Figure 37*** *¹H NMR spectra of A2*

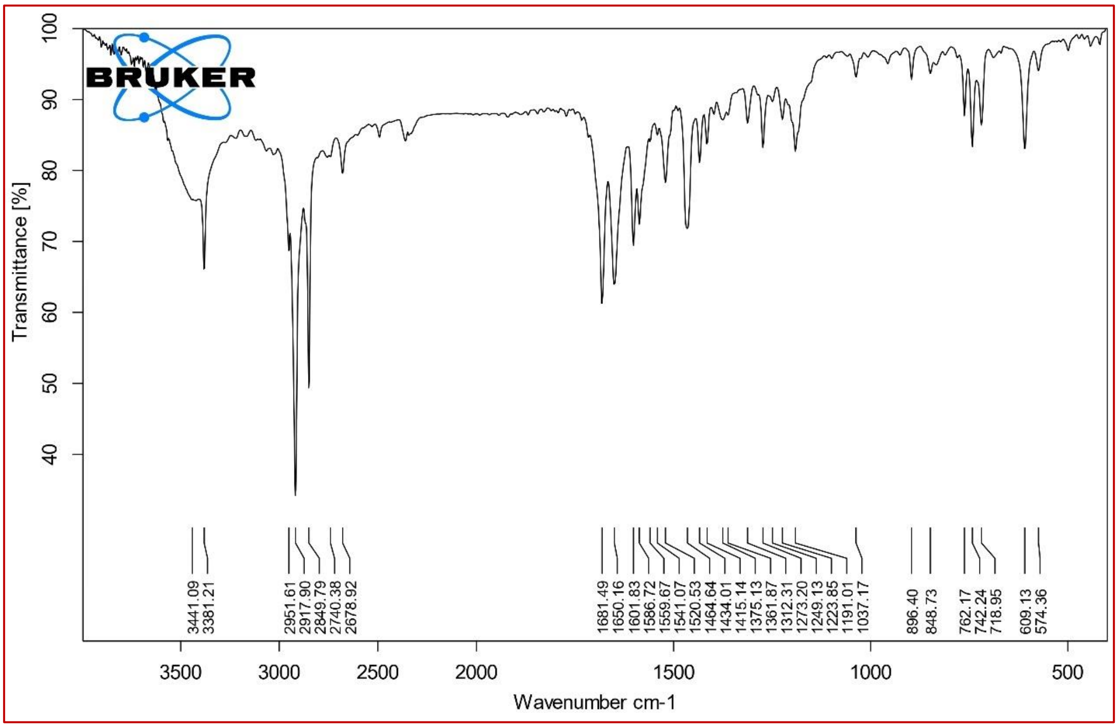


*Figure 38 IR spectra of A2*

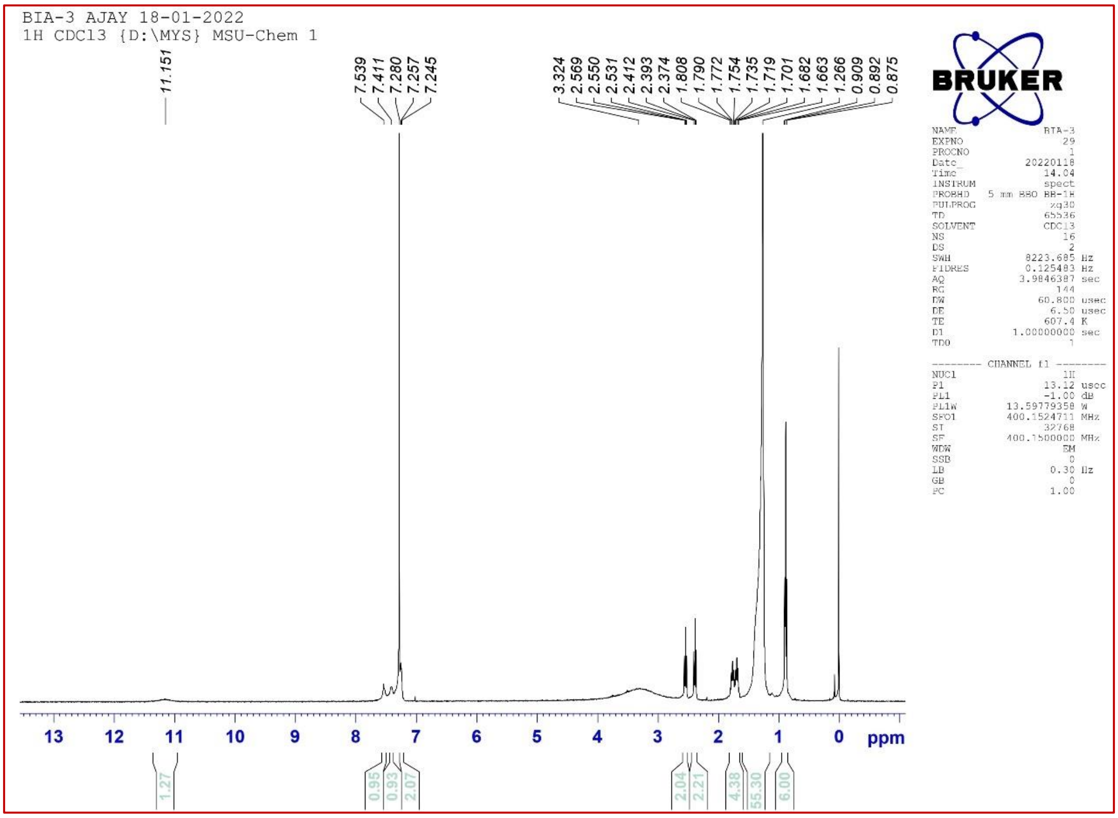


*Figure 39* [1]*H NMR spectra of A3*

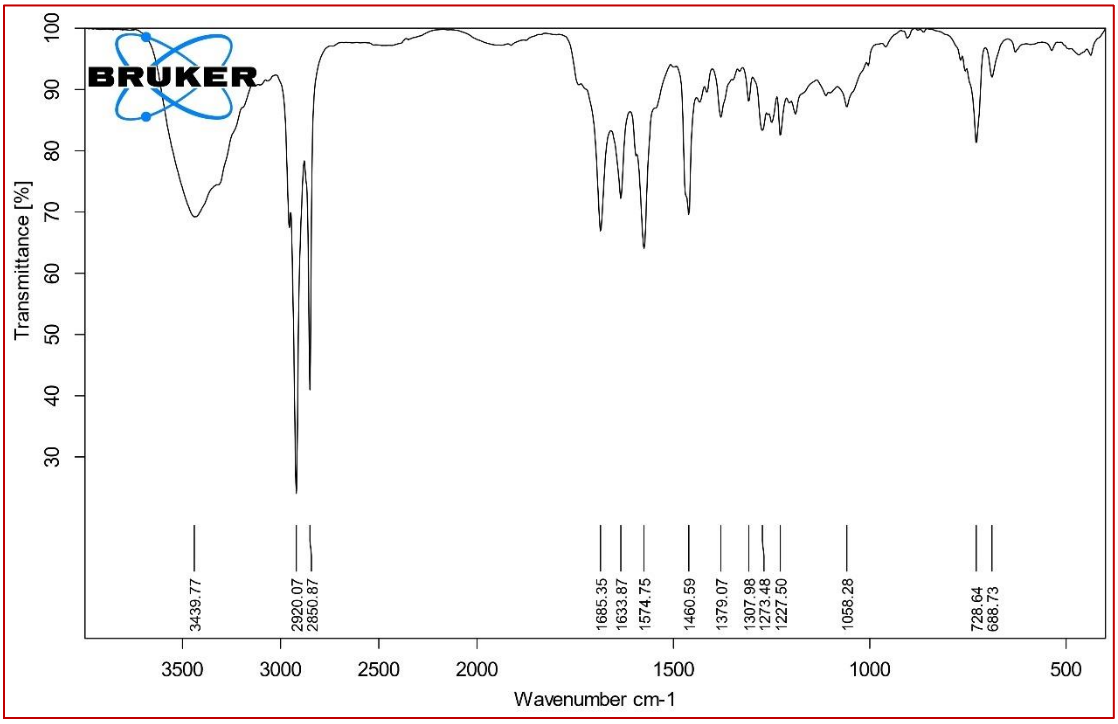


***Figure 40*** *IR spectra of A3*

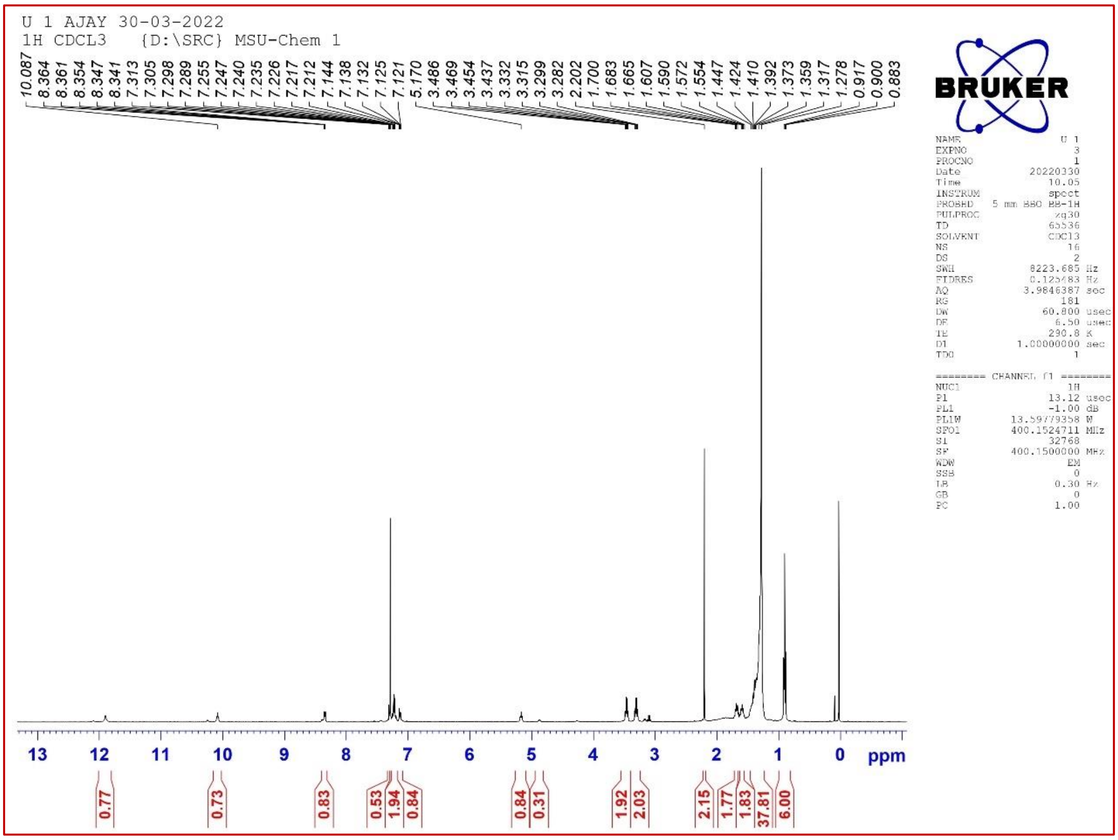

***Figure 41*** *[1]H NMR spectra of U1*

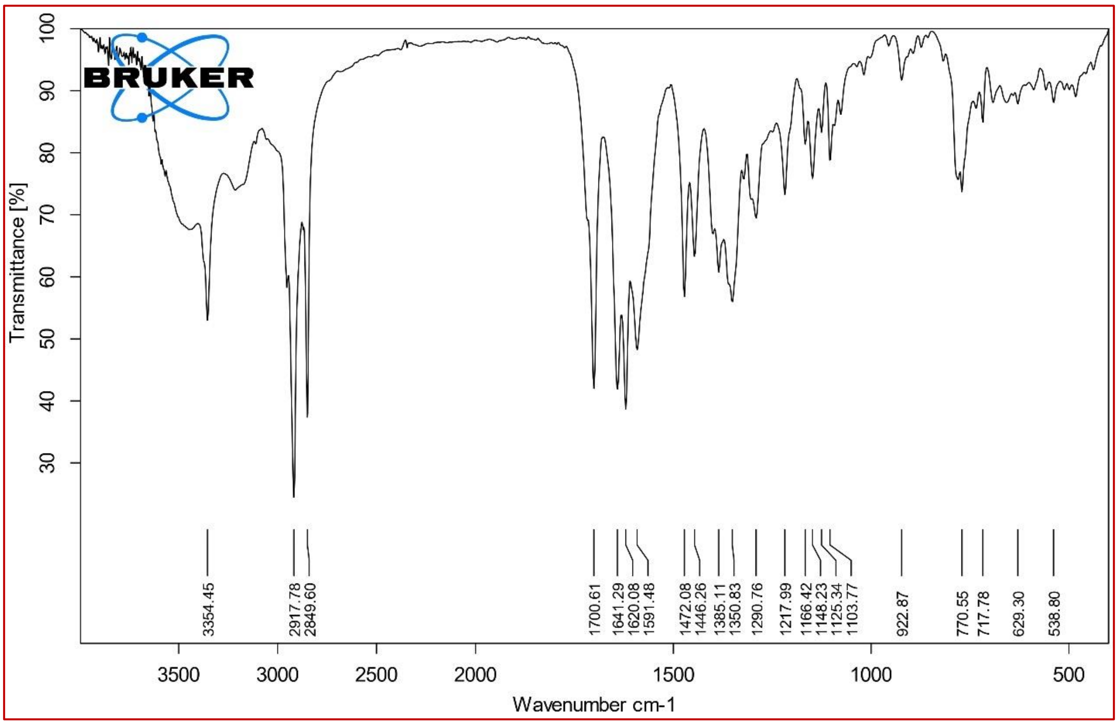

***Figure 42*** *IR spectra of U1*

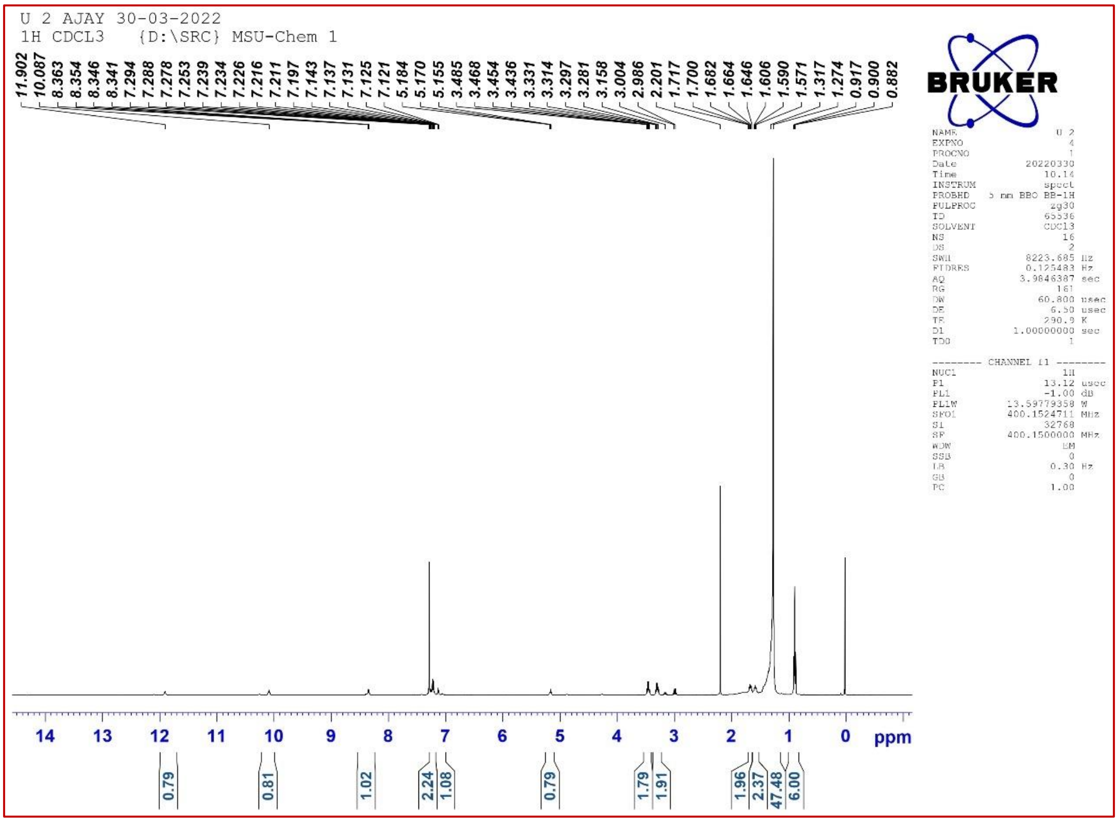


***Figure 43*** *[1]H NMR spectra of U2*

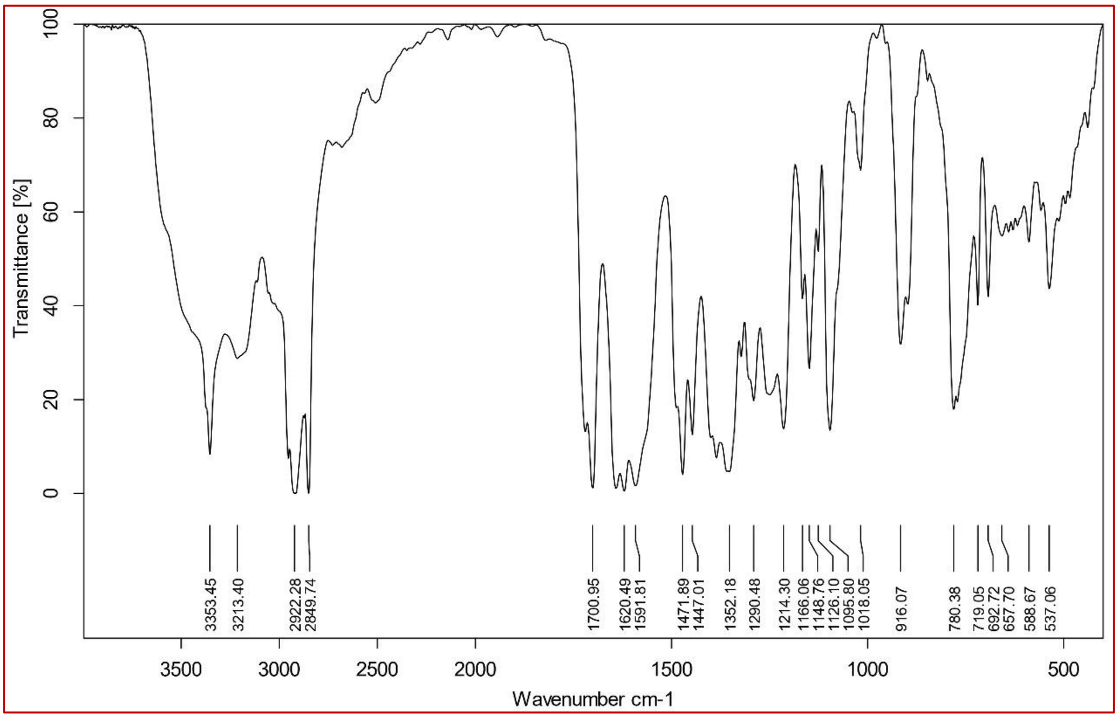


***Figure 44*** *IR spectra of U2*

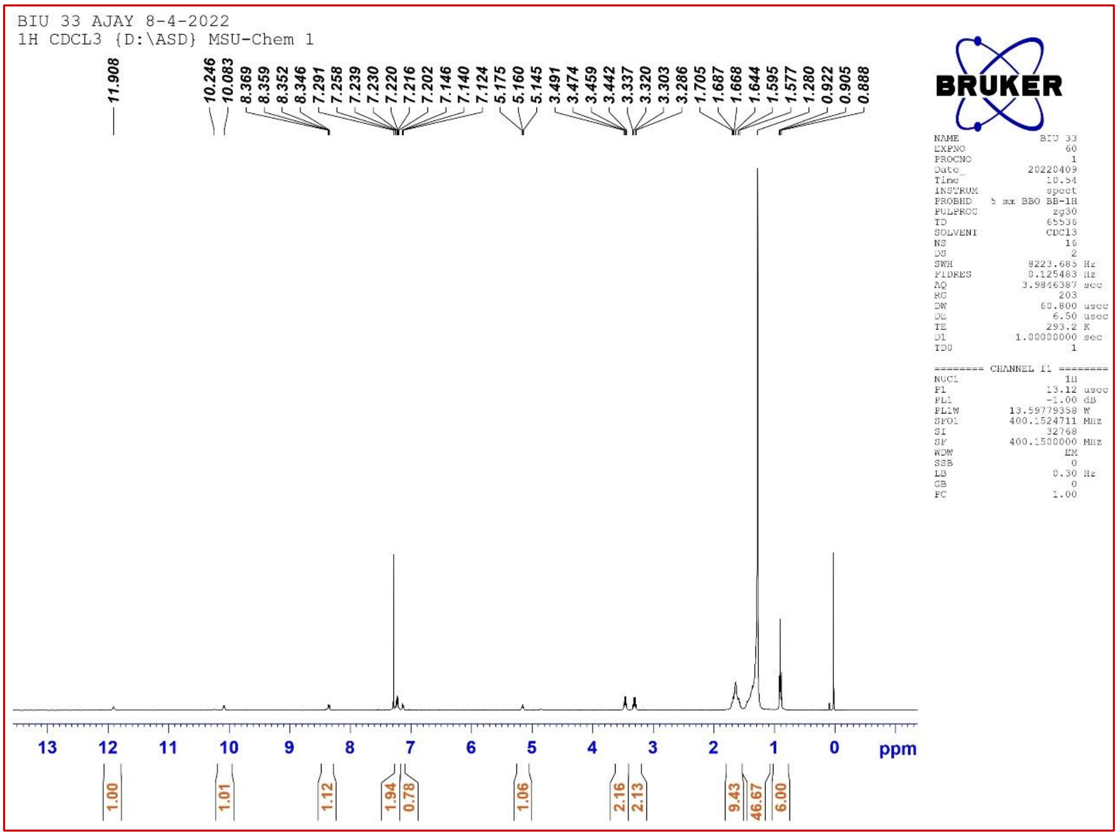

*Figure 45* ¹H NMR spectra of U3

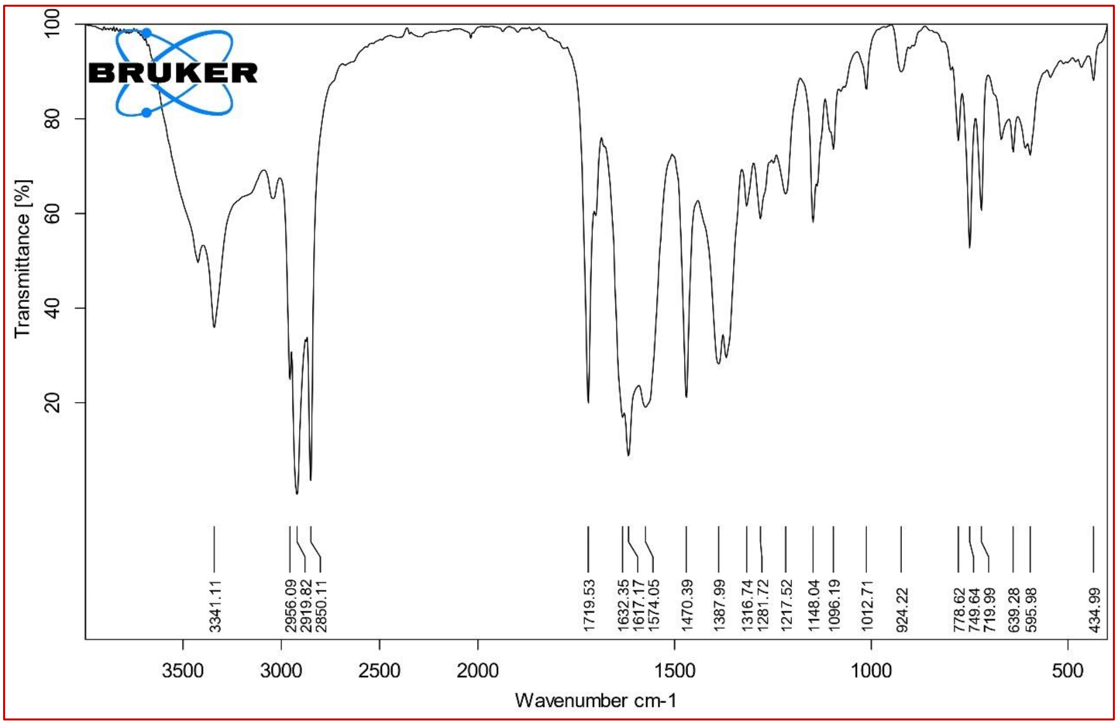

*Figure 46* IR spectra of U3

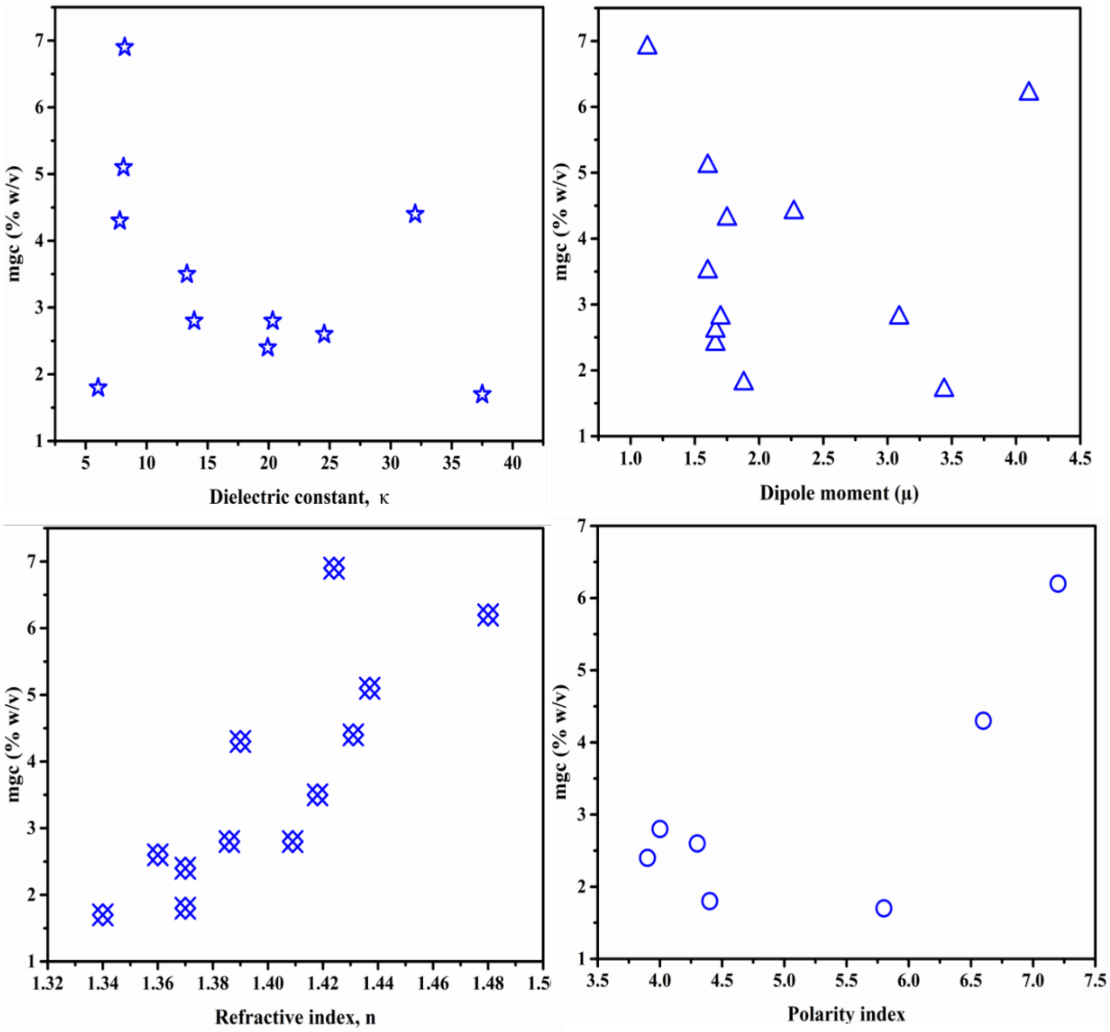


***Figure 47*** *Variation of mgc values with dielectric constants, dipole moments, refractive indices and polarity indices of the solvents for A1*

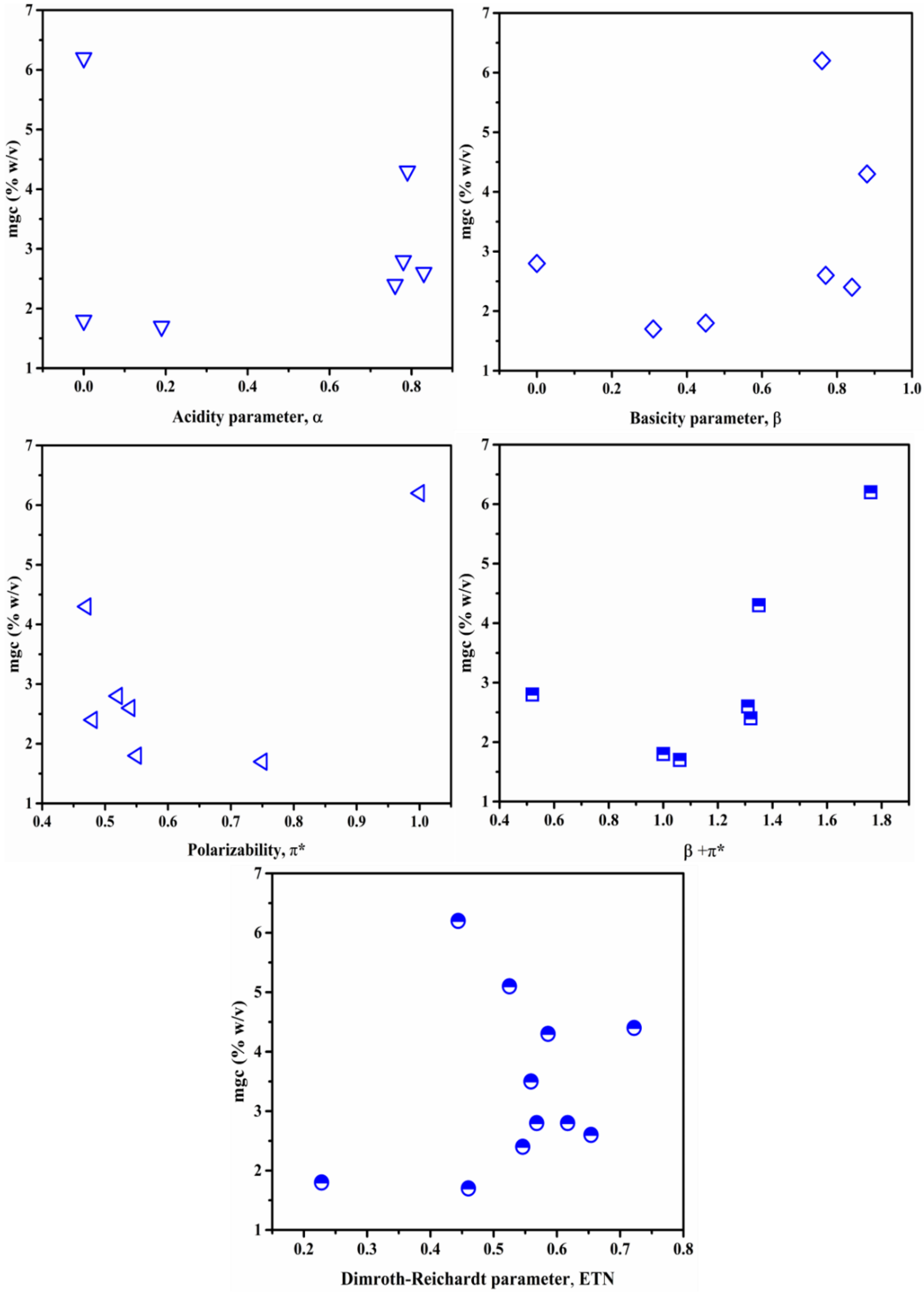


***Figure 48*** *Variation of mgc values with acidity and basicity parameters, polarizibilty and Normalized Dimroth-Reichardt parameters of the solvents for A1*

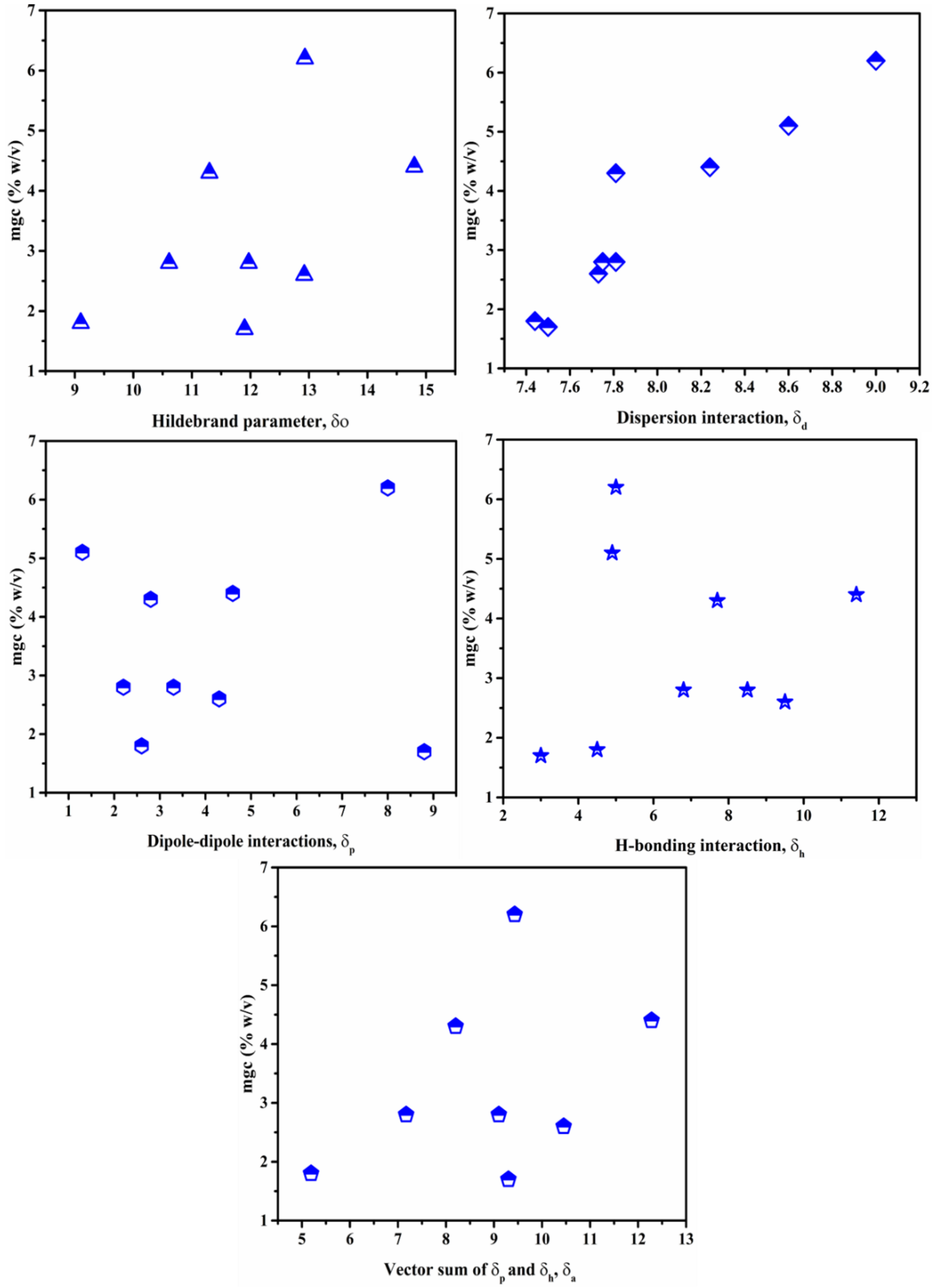


***Figure 49** Variation of mgc values with thermodynamically derived solvent parameters for A1*

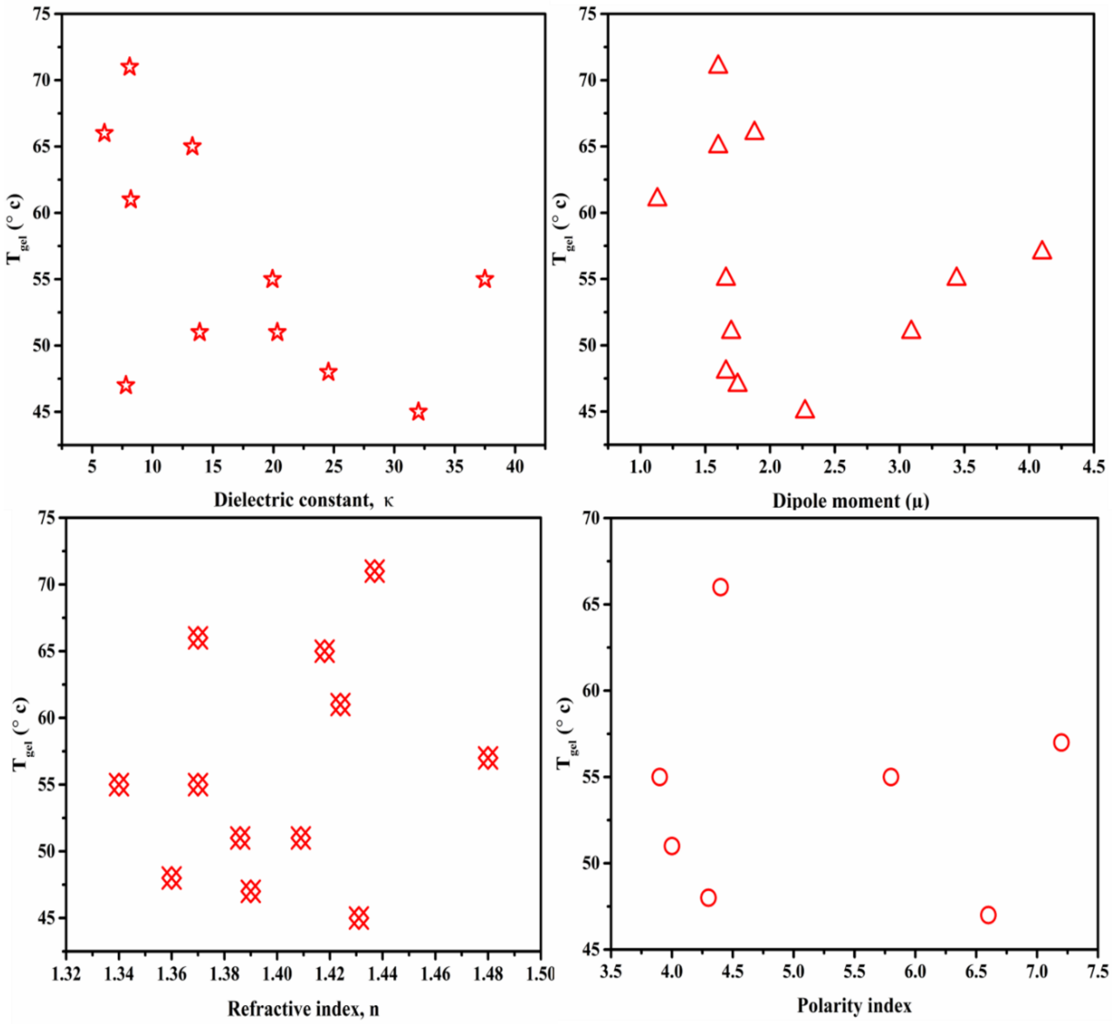


*Figure 50 Variation of $T_{gel}$ values with dielectric constants, dipole moments, refractive indices and polarity indices of the solvents for A1*

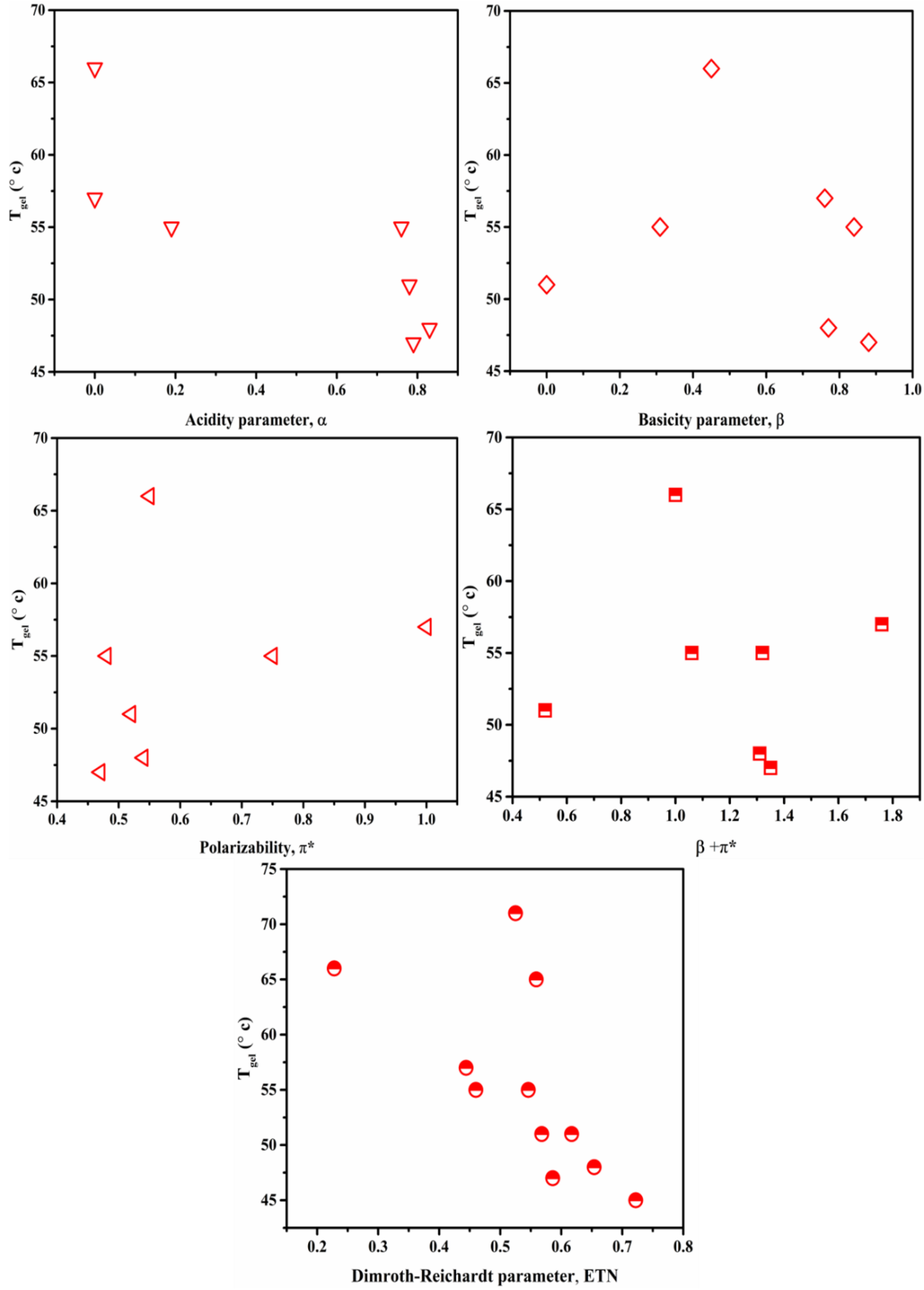


***Figure 51*** *Variation of $T_{gel}$ values with acidity and basicity parameters, polarizibilty and Normalized Dimroth-Reichardt parameters of the solvents for A1*

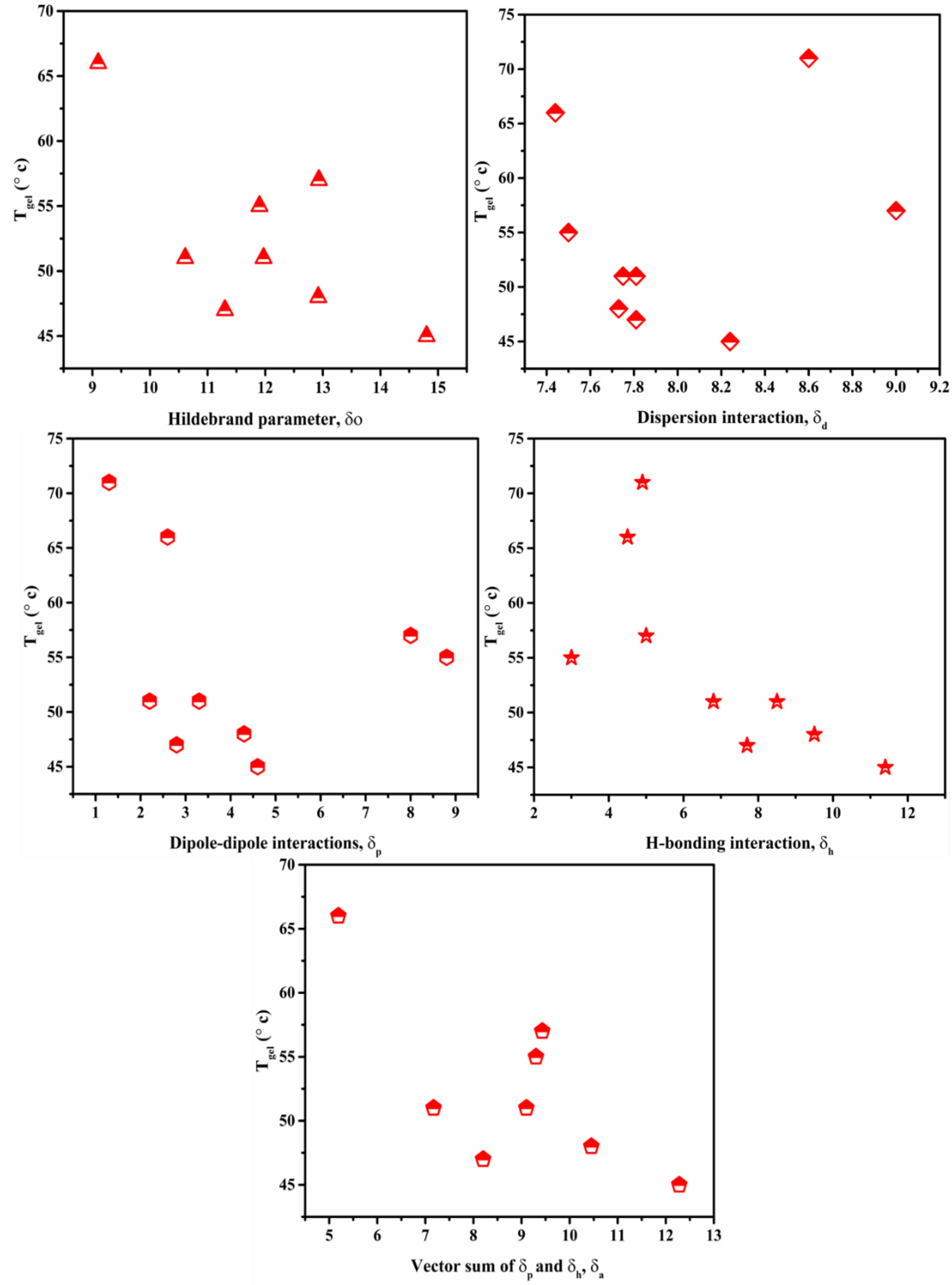


***Figure 52*** *Variation of $T_{gel}$ values with thermodynamically derived solvent parameters for A1*

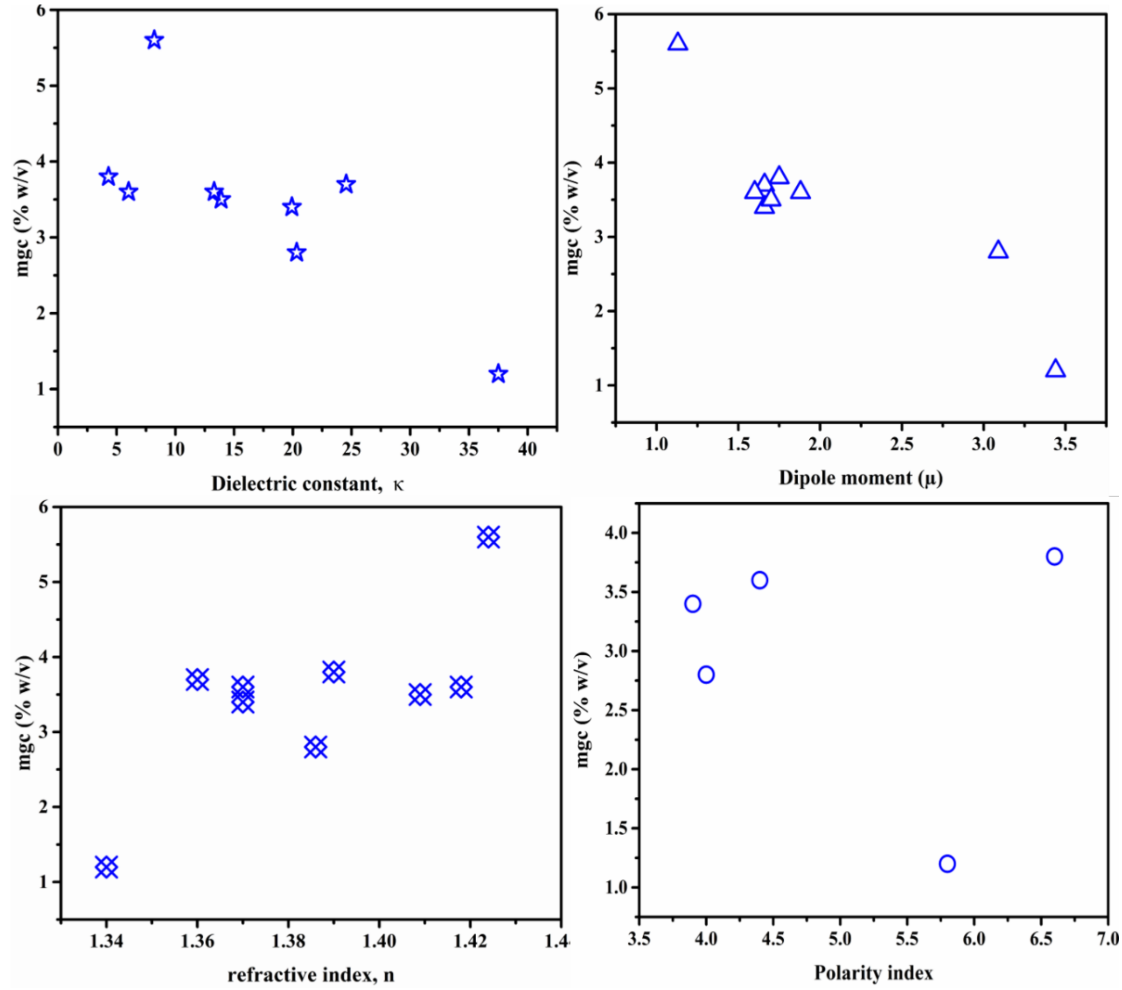


***Figure 53*** *Variation of mgc values with dielectric constants, dipole moments, refractive indices and polarity indices of the solvents for A2*

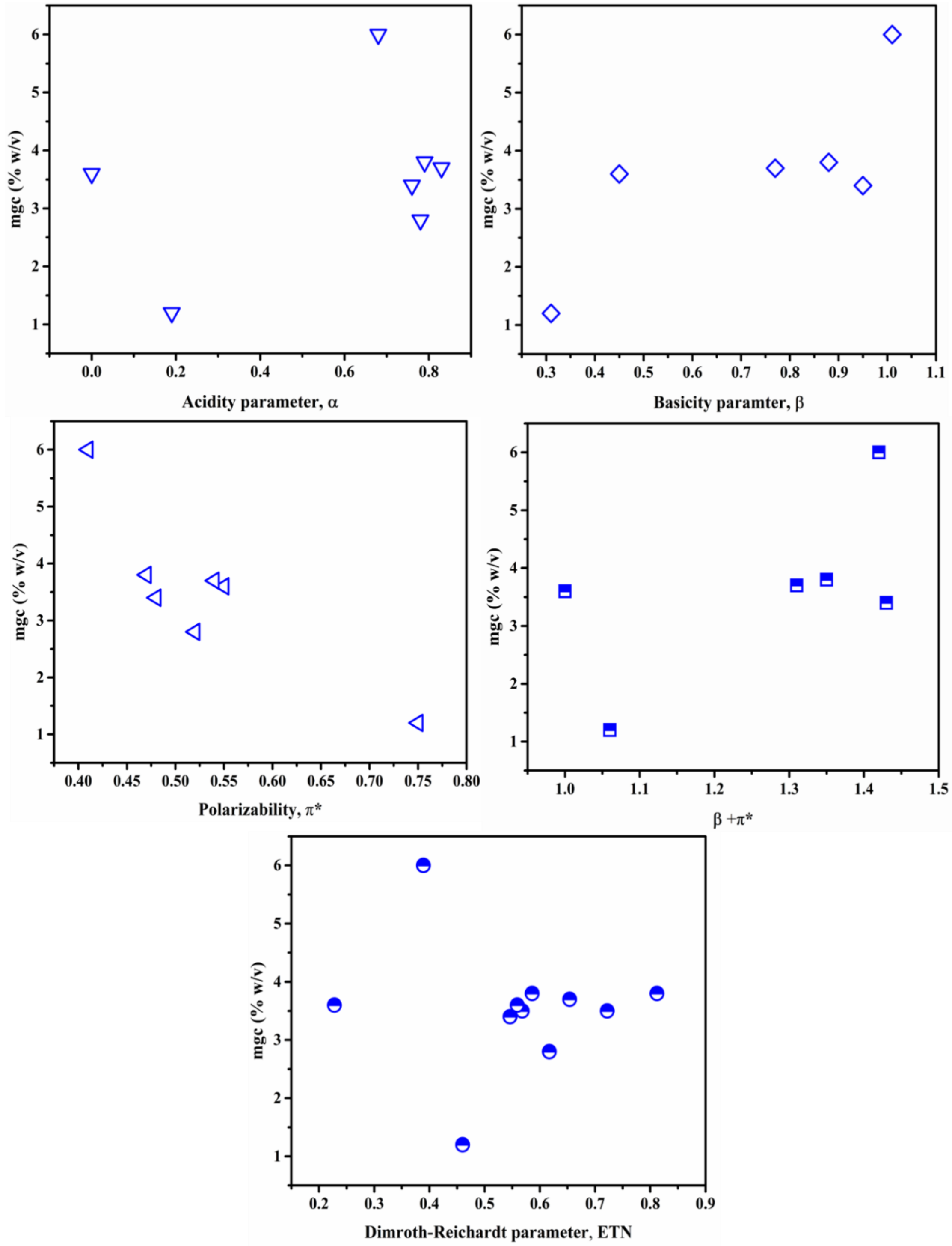


***Figure 54** Variation of mgc values with acidity and basicity parameters, polarizibilty and Normalized Dimroth-Reichardt parameters of the solvents for A2*

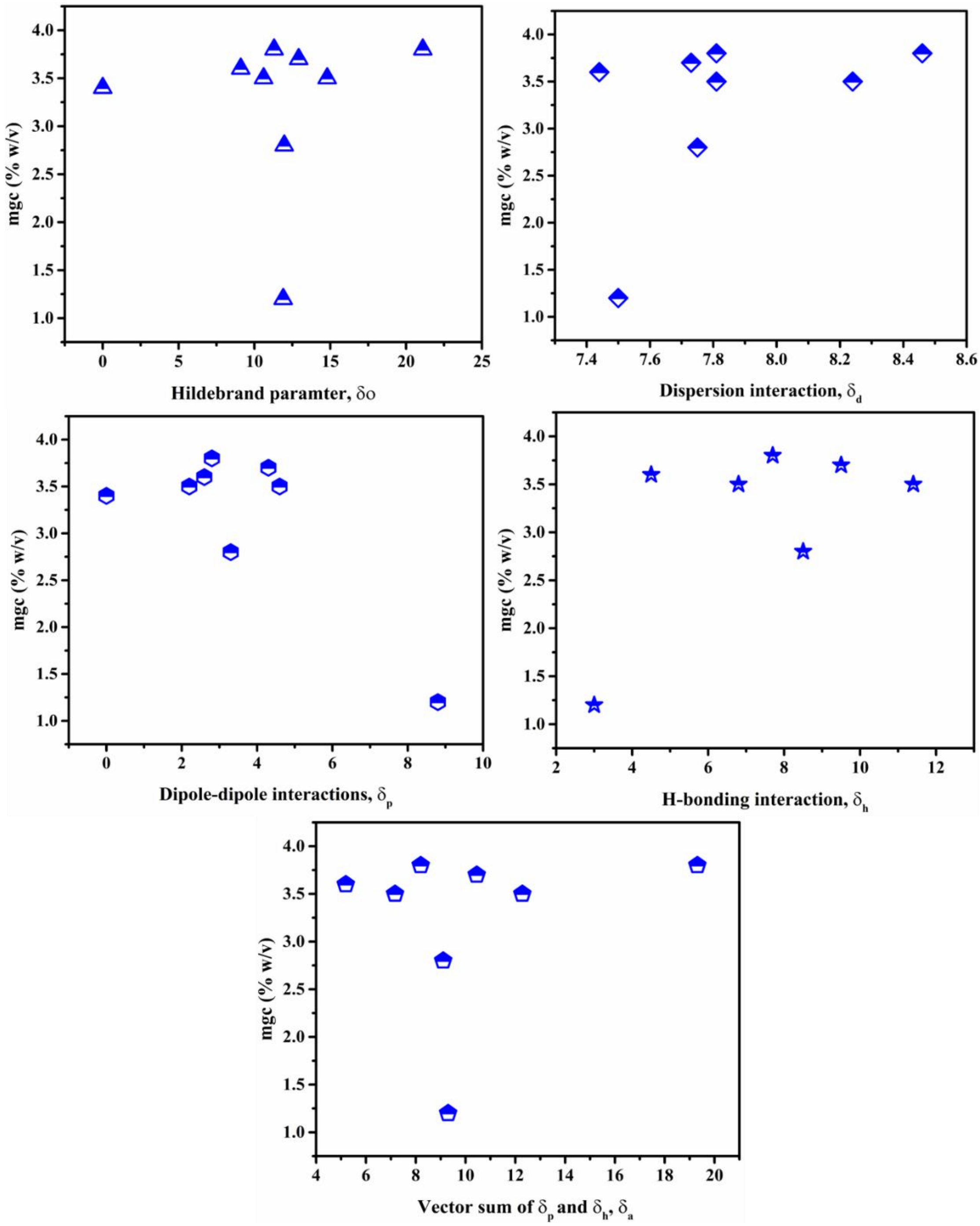


***Figure** 55 Variation of mgc values with thermodynamically derived solvent parameters for A2*

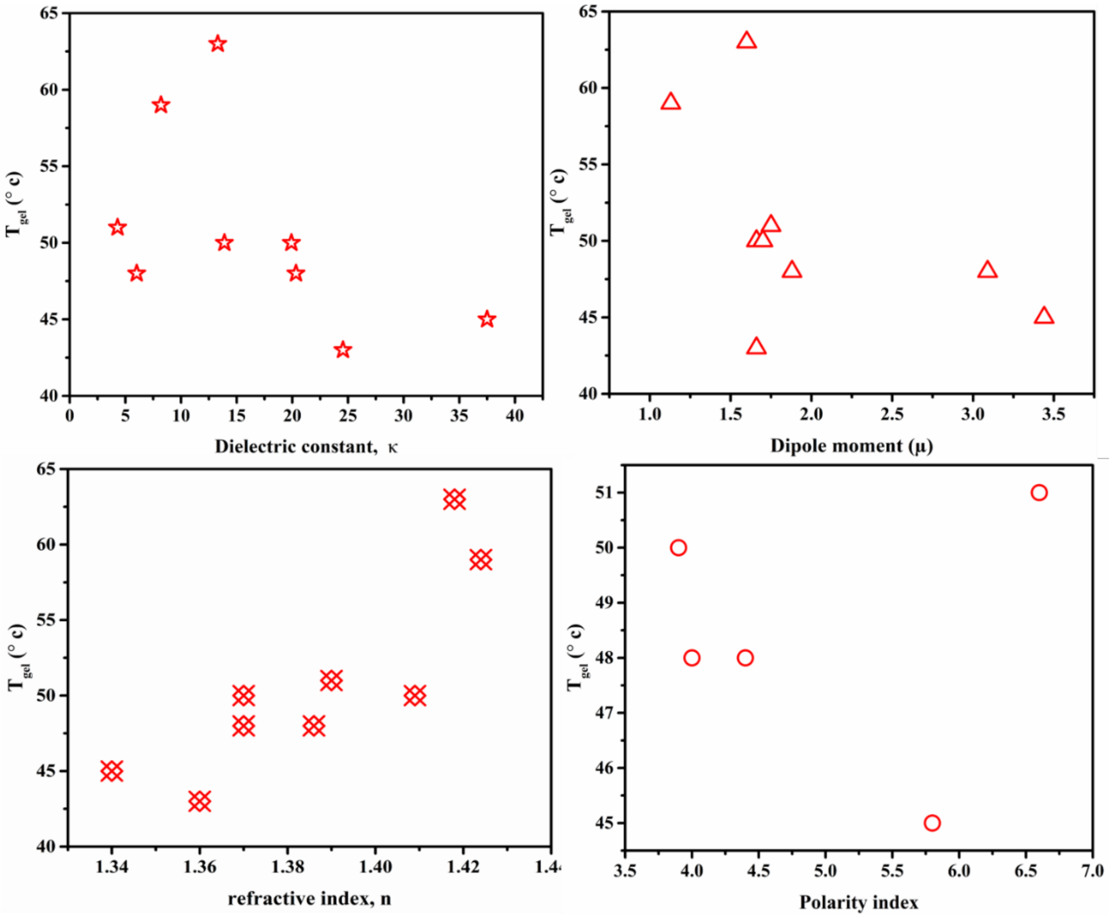


***Figure 56*** *Variation of $T_{gel}$ values with dielectric constants, dipole moments, refractive indices and polarity indices of the solvents for A2*

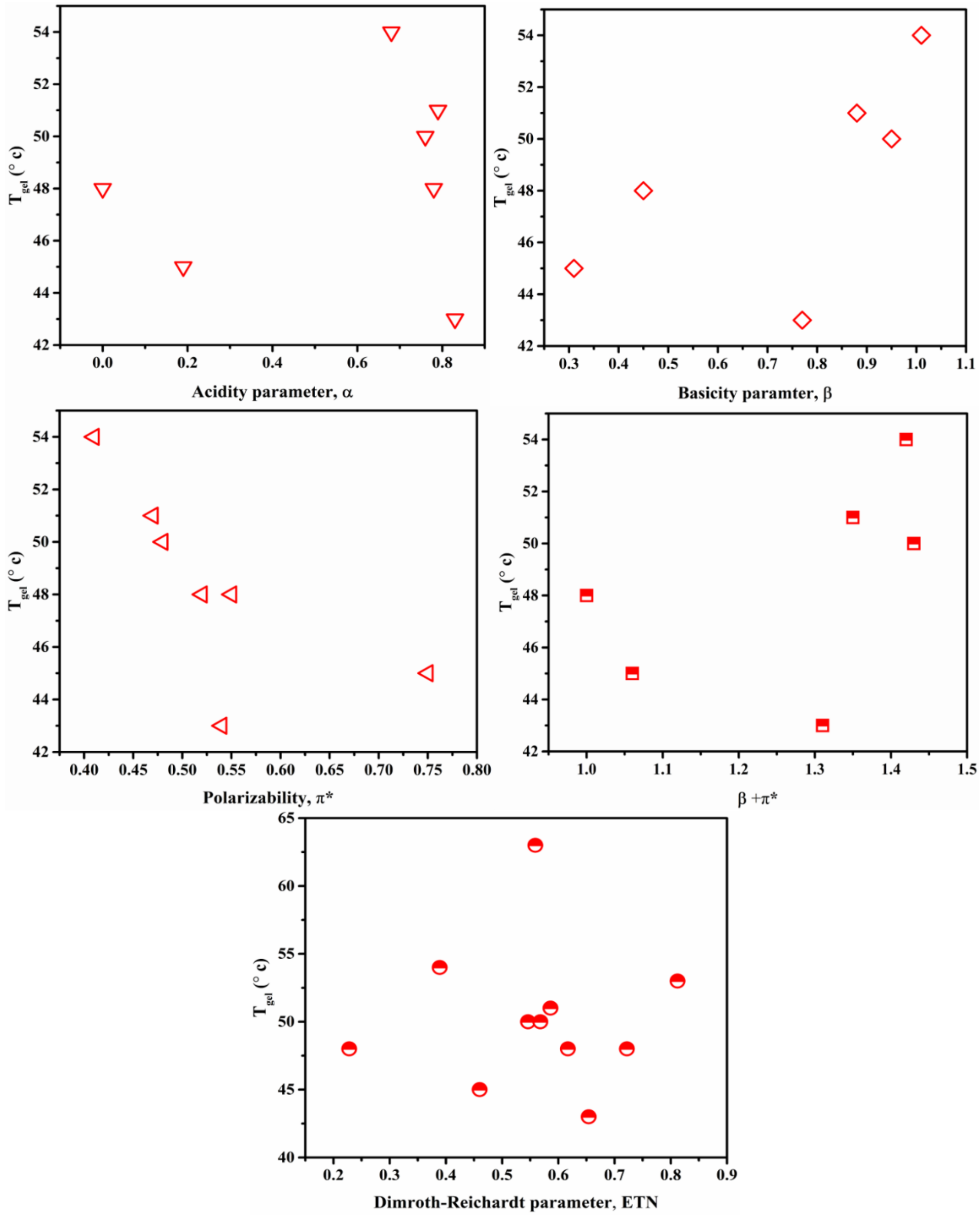


***Figure 57*** *Variation of $T_{gel}$ values with acidity and basicity parameters, polarizibilty and Normalized Dimroth-Reichardt parameters of the solvents for A2*

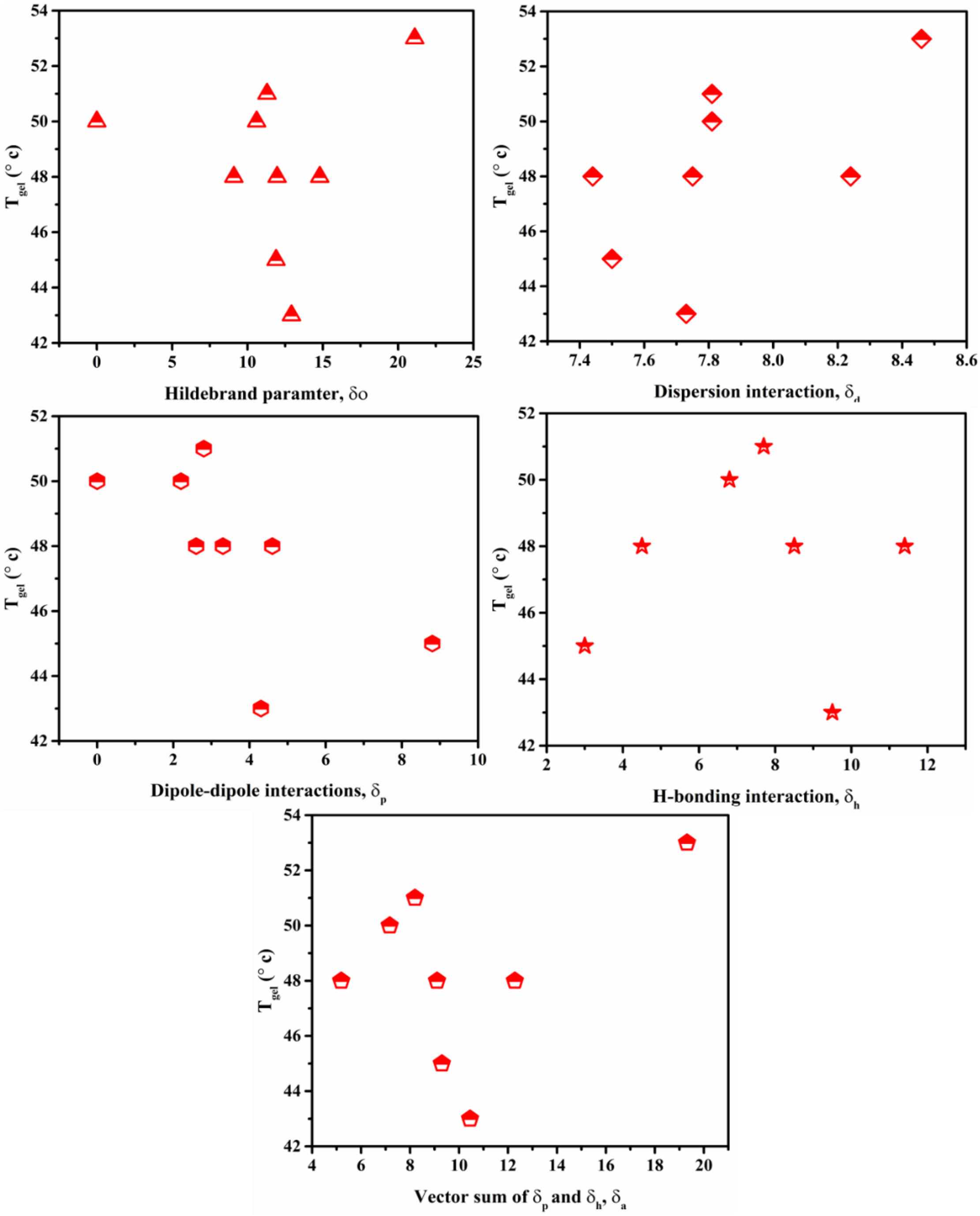


***Figure 58*** *Variation of $T_{gel}$ values with thermodynamically derived solvent parameters for A2*

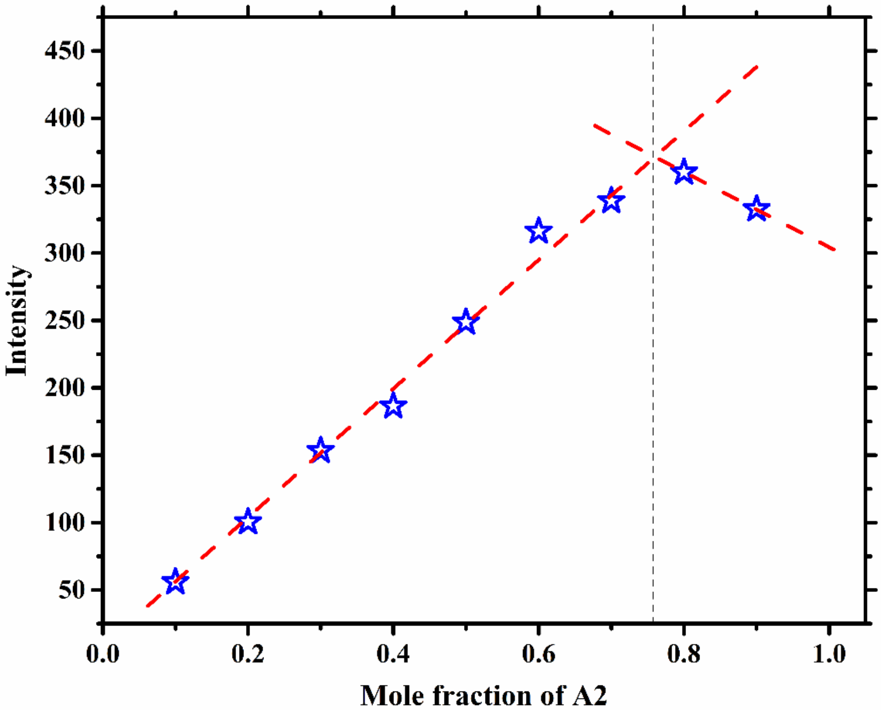


***Figure 59*** *Jobs plot of A2*

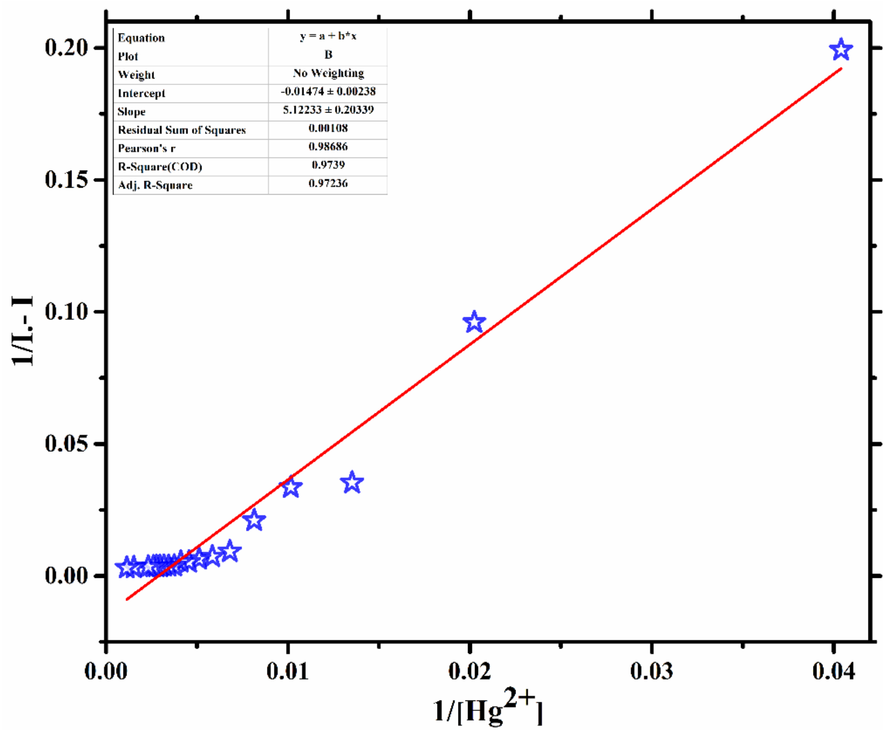


***Figure 60*** *Limit of detection of A2*

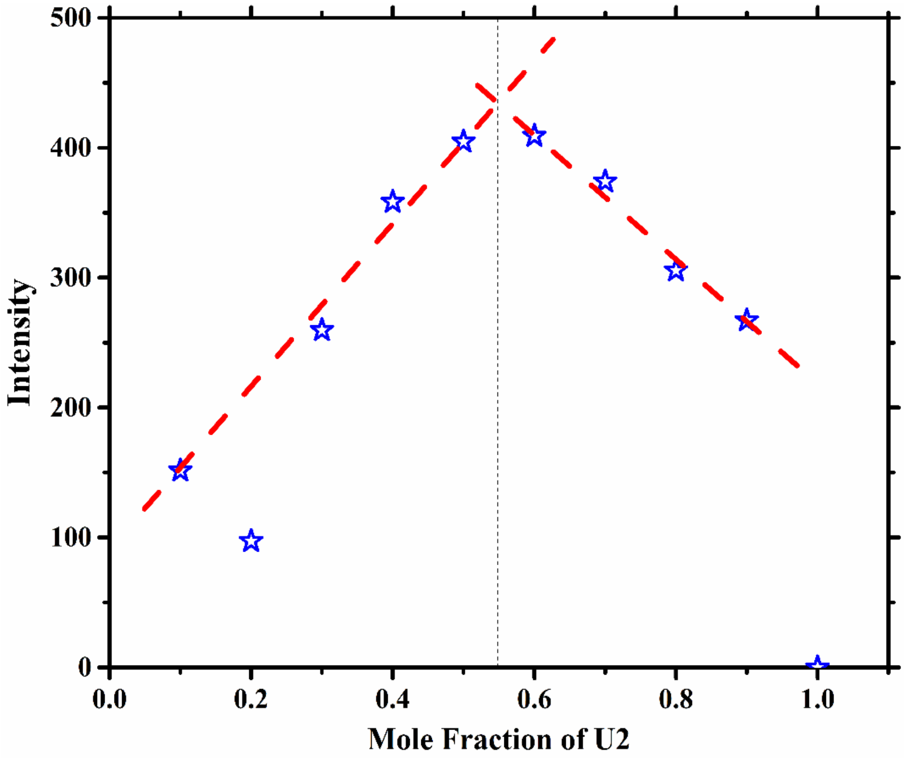


*Figure 61* Jobs plot of U2

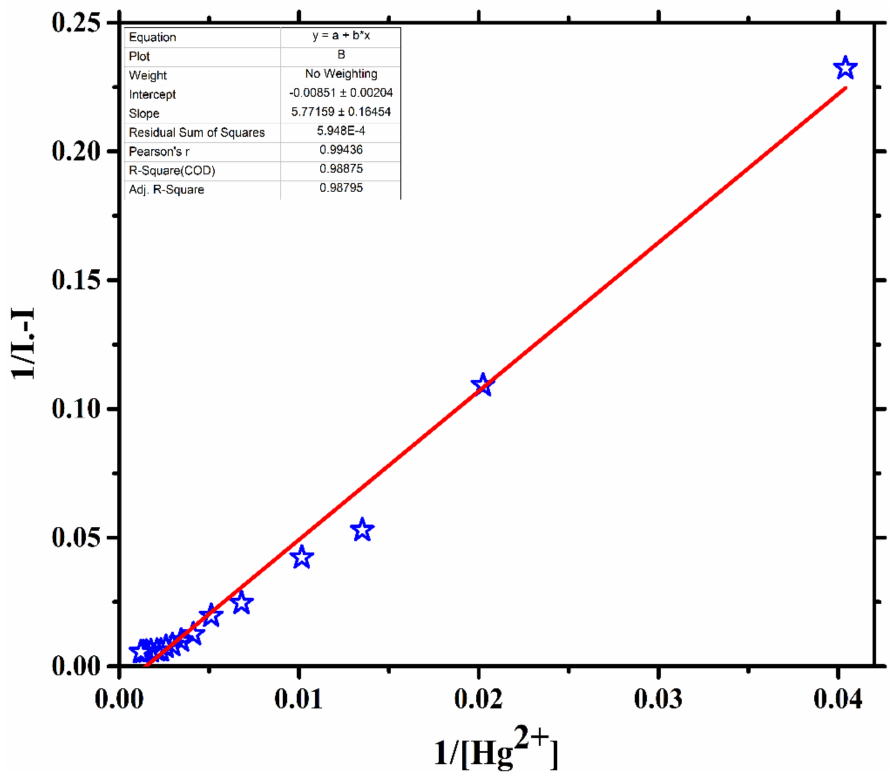


*Figure 62* Limit of detection od U2